BL7B

Optical Pseudogap from Iron States in AFe$_4$Sb$_{12}$ (A=Yb, Ca, Ba)

J. Sichelschmidt[1], H.J. Im[2,3], S. Kimura[2,3], V. Voevodin[1], H. Rosner[1], W. Schnelle[1], A. Leithe-Jasper[1], J.A. Mydosh[1,4], Yu. Grin[1], F. Steglich[1]

[1]*Max Planck Institute for Chemical Physics of Solids, 01187 Dresden, Germany*

[2]*School of Physical Sciences, The Graduate University for Advanced Studies, Okazaki 444-8585 Japan*

[3]*UVSOR Facility, Institute for Molecular Science, Okazaki 444-8585 Japan*

[4]*II. Physikalisches Institut, Universität zu Köln, 50937 Köln, Germany*

Introduction

The class of compounds known as "skutterudites" exhibits a wealth of topical behaviors. A variety of properties have been observed – mainly for rare-earth filled skutterudites – ranging from metal-insulator transitions to magnetic and quadrupole orderings, conventional and unconventional superconductivity, heavy-fermion/non-Fermi-liquid behavior, and fluctuating/intermediate valency. Many studies suggest that the physics of filled skutterudites with rare-earth metals is governed by a subtle interplay of the filler ions and their surrounding transition-metal pnictogen host structure.

The skutterudites AFe$_4$Sb$_{12}$ filled by nonmagnetic ions of alkali and alkaline-earth metals show remarkable properties which indicate the importance of magnetism originating in the polyanionic host [1,2]. These compounds either show ferromagnetic ordering (A = Na, K) or are close to a ferromagnetic instability (A = Ca, Ba). Strong ferromagnetic spin fluctuations, a high density of states (DOS) at the Fermi level E_F and, therefore, an enhanced electronic specific heat coefficient $\gamma \approx$ 100-140 mJ mol^{-1}K^{-2} are found [2,3]. Thus, with respect to these new findings the size of the contribution of the 4f-conduction electron hybridization to the creation of an enhanced/heavy effective electronic mass in some rare-earth filled iron skutterudites becomes questionable. In YbFe$_4$Sb$_{12}$ the Yb is non-magnetic and stable divalent as recently proven experimentally [3,4]. In contrast, previous optical investigations of YbFe$_4$Sb$_{12}$ claim 4f -related heavy fermion properties reflected in a hybridization induced far-infrared (FIR) pseudogap [5]. We clarified the nature of this pseudogap by comparing the optical properties of YbFe$_4$Sb$_{12}$ with those of (Ca/Ba)Fe$_4$Sb$_{12}$. We found a low-energy pseudogap structure, very similar for each compound. It reflects the fine details of the band structure near E_F which can be understood in a single particle picture without including explicitly electron-electron correlations [6]. The Fe-3d states generate the observed pseudogap whose characteristics appears to be very similar to the so-called hybridization gap found in some strongly correlated 4f electron systems.

Experiment

We have measured the near normal incidence optical reflectivity $R(\omega)$ of polycrystalline samples of AFe$_4$Sb$_{12}$ (A = Yb, Ca, Ba). Their preparation and structure as well as their transport, thermodynamic, and magnetic properties were reported previously [1-3]. For the optical experiments the sample surfaces were well polished.

A rapid-scan Fourier spectrometer of Michelson and Martin-Puplett type was used for energies $\hbar\omega$ between 3 meV and 3 eV (2 K< T < 300 K) and for higher energies at T = 300 K only. Synchrotron radiation (UVSOR, BL7B) extended the energy range from 1.2 eV up to 30 eV [7]. As high accuracy for the reflection data was required, the polycrystalline samples were coated *in-situ* with gold and then used for measuring the reference spectra. Using Kramers-Kronig relations, we calculated the dissipative part $\sigma_1(\omega)$ of the optical conductivity from $R(\omega)$. Above energies of 30 eV, where an eventual small temperature dependence of $R(\omega)$ has negligible influence on $\sigma_1(\omega \approx 10$ meV), a free-electron approximation of the form $R(\omega) \propto \omega^{-4}$ was used. We fitted the low-energy end $\sigma_1(\omega \leq 30$ meV) to the electrical conductivity σ_{DC} ($\omega \rightarrow 0$) by a Drude-Lorentz function such that σ_{DC} values were described within ±20%. Uncertainties of the $\sigma_1(\omega)$ spectra due to variations of the low-energy extrapolation of $R(\omega)$ are negligible for energies > 6 meV.

Results

The measured reflectivity spectra $R(\omega,T)$ data are shown in Fig. 1 at selected temperatures. A sharp drop of $R(\omega)$ around 0.5 eV separates a Drude-like charge carrier contribution at low energies from electronic interband transitions dominating the high-energy region (see inset). Below $T \approx$ 90 K $R(\omega)$ shows a pronounced suppression of up to ≈ 4% (T = 4 K) with a minimum located at about the same energy (12 meV) for CaFe$_4$Sb$_{12}$ and YbFe$_4$Sb$_{12}$, and at ≈ 15 meV for BaFe$_4$Sb$_{12}$. The compounds show conventional metallic behavior in the optical conductivity $\sigma_1(\omega,T)$ above $T \approx$ 90 K whereas for T < 90 K it is continuously suppressed until it reaches a minimum value at the lowest temperature. This behavior of $\sigma_1(\omega,T)$ and its enhancement for energies between 17 and 60 meV indicates the formation of a pseudogap in the electronic charge excitations below ≅ 17 meV (see Fig. 2).

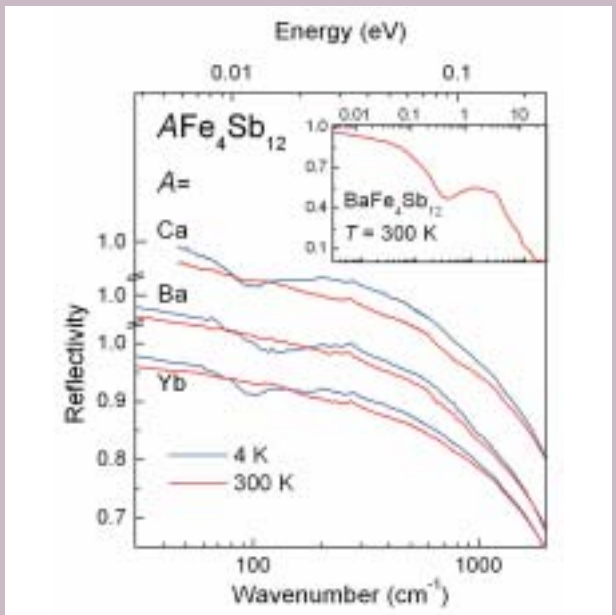

Fig. 1 Reflectivity spectra displaying for all compounds at $T = 4$ K a pronounced dip around 100 cm^{-1}. Inset: the complete accessible spectral range shown for one compound.

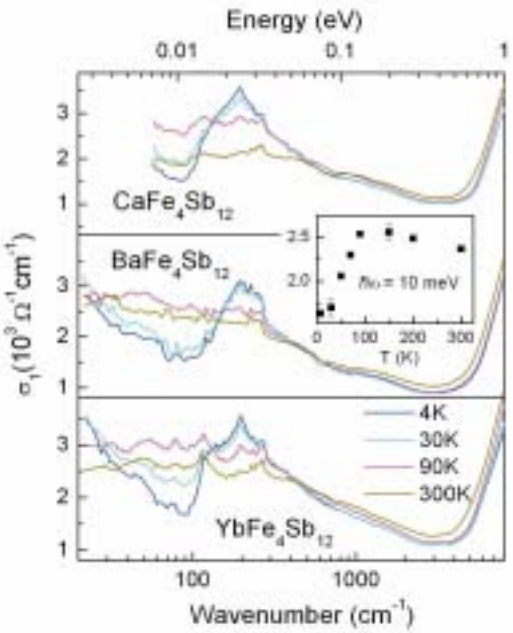

Fig. 2 Spectra of the optical conductivity $\sigma_1(\omega,T)$ at selected temperatures below and above $T \approx 90$ K, where a pseudogap forms below 17 meV. For $BaFe_4Sb_{12}$ the inset shows $\sigma_1(\omega,T)$ at $\hbar\omega = 10$ meV, demonstrating the evolution of the pseudogap.

Remarkably, all investigated compounds AFe_4Sb_{12} (A = Yb, Ba, Ca) show a very similar pseudogap behavior of their optical conductivities, pointing towards a very similar electronic band-structure. Indeed, the optical pseudogap and its different appearances in $BaFe_4Sb_{12}$ and $CaFe_4Sb_{12}$ as well as the sharp features (for example close to 200 cm^{-1}) are very well reproduced by our high-resolution LDA band-structure calculations [6]. Therefore, at least for AFe_4Sb_{12} with A = Yb, Ca, Ba only weak electronic correlations within the Fe 3*d* – Sb 5*p* bands seem to be present. This is a completely different mechanism than the Kondo-insulator gap scenario for 4*f* heavy-fermion compounds leading, surprisingly however, to similar optical spectra.

Keeping in mind the relevance claimed for the hybridization gap picture in other filled skutterudites [5,8] our results, with unexpected clearness, demonstrate that FIR optical pseudogaps can originate from the single particle electronic band structure of these systems.

This work was partially supported from the international collaboration program of IMS (2004).

[1] A. Leithe-Jasper *et al.*, Phys. Rev. Lett. **91** (2003) 037208.
[2] A. Leithe-Jasper *et al.*, Phys. Rev. B **70** (2004) 214418.
[3] W. Schnelle *et al.*, Phys. Rev. B **72** (2005) 020402(R).
[4] D. Bérardan *et al.*, J. Alloys Compd. **351** (2003) 18; *ibid.* J. Magn. Magn. Mater. **285** (2005) 245.
[5] S. Dordevic *et al.*, Phys. Rev. Lett. **86** (2001) 684.
[6] J. Sichelschmidt *et al.*, Phys. Rev. Lett **96** (2006) 037406.
[7] K. Fukui *et al.*, Nucl. Instrum. Methods Phys. Res. Sect. A **467-468** (2001) 601.
[8] M. Matsunami *et al.*, J. Phys. Soc. Jpn. **72** (2003) 2722.

BL1A, 5B, 7B&8B1

Photo Luminescence Spectra and Time Resolved Decay Curves of UV Emission Bands in AlGaN Alloys Using High Energy Excitation

S. Naoe[1], N. Nakagawa[2], K. Fukui[2], H. Miyake[3], K. Hiramatsu[3]
[1]*Faculty of Engineering, Kanazawa University, Ishikawa 920-1192, Japan*
[2]*Research Center for Development of Far-Infrared Region, Fukui 910-8562, Japan*
[3]*Faculty of Engineering, Mie University, Mie 514-8507, Japan*

AlGaN is becoming an important optical material which gives UV emission band with variable energy position from 3.4 to 6.25 eV, therefore the study of mechanism of UV emission in the photoluminescence measurements by using SR in wide energy range of exciting photon is expected.

All samples are made by MOCVD (MOVPE) methods. The thicknesses of AlGaN thin film are about 1 μm on 1 μm AlN single crystal films with sapphire substrates. The measurements were carried out at BL1A, under single bunch operation to take of time resolved decay (TRD) curves.

TRD curves have three components (fast < 1 ns, middle ~18 ns, slow ~60 ns) by analyzing based on the three single exponential components linear combination model. Previous works revealed that the rate of the fast component among them increases with increasing excitation photon energy up to 1.5 keV in TRD curves of AlGaN [1]. This time, TRD measurements were done for sliced parts of UV emission band with the precision of receiving light monochromator resolving power (0.02 eV), using various energy ranges of excitation photon (BL7B, BL5B, BL8B1, BL1A). Thus, it gives life time resolved PL spectra.

In the case of band-to-band excitation (BL7B), the rates of three components of TRD have shown to vary with changing the detected photon energy value of the sliced parts among the UV emission band (this result will be reported elsewhere in this article).

In the case of high energy excitation (BL1A), where the fast component was known to become dominant in TRD curve for the whole of UV emission band, the behavior of the rate of three components in the life time resolved PL spectra is interesting , varying the energy of detecting photon among the UV emission band.

The results of TRD measurements at low temperature are shown in Fig. 1 and Fig. 2. Fig.1 shows UV emission band and the inserted color points show the position of detecting photon energy in TRD measurement. Fig.2 shows TRD curves at several energy position of photon detected. There is no considerable difference at the energy values (corresponding to the color points in Fig. 2) among the UV emission band, in contrast to the case of band-to-band excitation (BL7B).

These TRD results will be interpreted by the relaxation process of some holes and electrons produced by the high energy excitations, on the UV emission. The fast component will be considered to originate from an intrinsic exciton process (overlapping between electron and hole wave functions), then it will be suggested as a schematic view that many holes which were produced by relaxation process of inner core holes are gathering around the element initially excited and recombining with nearby electrons rapidly, before making some relaxation state.

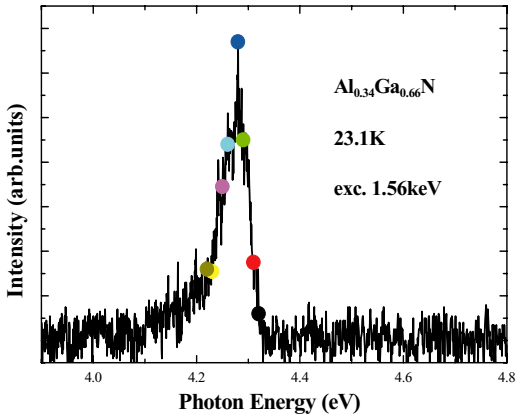

Fig. 1 UV emission band of $Al_{0.34}Ga_{0.66}N$ at 23.1K.

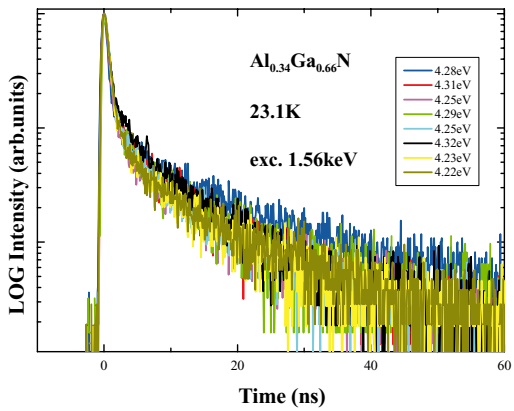

Fig. 2 Time resolved decay curves of $Al_{0.34}Ga_{0.66}N$ at 23.1K.

[1] S. Naoe *et al.,* UVSOR Activity Report 2004, (2005) 78.

BL1B

Luminescence Properties of $NaYF_4:Bi^{3+}$

K. Chong[1], T. Hirai[1], T. Kawai[2], N. Ohno[1]

[1]*Division of Electronics and Applied Physics, Graduate School of Engineering, Osaka Electro-Communication University, Neyagawa, Osaka 572-8530, Japan*

[2]*Graduate School of Science, Osaka Prefecture University, Sakai 590-0035, Japan*

Xe dimer (Xe_2) discharge fluorescent lamp is one of the candidates for alternative lighting sources to a conventional Hg discharge fluorescent lamp. New phosphors suitable for the conversion of vacuum ultraviolet (VUV) light into visible light are quite desired at present. In the Xe_2 discharge florescent lamps, phosphors are excited by VUV light at 7.2 eV. Most fluoride hosts are transparent up to ~ 10 eV, so that the VUV light can directly excite impurity activators in fluoride hosts.

Metal ions with s^2 electronic configurations doped in wide-gap materials such as alkali halides, which are called Tl^+-type ions, show several absorption bands due to $s^2 \rightarrow sp$ transitions. Since the optical transitions are dipole-allowed, the absorption is expected to be much stronger than that due to the dipole- forbidden *f-f* transitions in rare-earth ions. The strong absorption would give efficient conversion of the VUV light from the Xe_2 discharge fluorescent lamps.

$NaYF_4:Bi^{3+}$ samples were prepared by amounts of the appropriate starting compound powders of NaF and YF_3 adding BiF_3 (~ 1 mol %), mixing and firing in a carbon crucible at 850ºC in argon atmosphere. X-ray diffraction patterns showed that obtained crystals were of a hexagonal structure. Impurity Bi^{3+} ions are trivalent Tl^+-type ions, so that they would be substituted for Y^{3+} ions in the host lattices.

Figure 1 shows PL (blue curve) and PLE (red curve) spectra of $NaYF_4:Bi^{3+}$ measured at 10 K. A broad luminescence band peaking at 2.75 eV is observed for the excitation of VUV light. The 2.75 eV band is excited with photons of 5.0 eV in the UV region, and ~ 6.2 eV in the VUV region. These excitation peaks are located at lower energies than the absorption edge of the host $NaYF_4$ (~ 8 eV). Therefore, the 2.75 eV luminescence band is responsible for intra-ionic transitions in impurity Bi^{3+} ions.

Tl^+-type ions doped in alkali halide crystals with a high symmetry crystal structure exhibit three characteristic absorption bands arising from the $s^2 \rightarrow sp$ transitions, namely, A, B and C bands [1]. These absorption bands have been attributed to the optical transition from the $^1S_0$ ground state to $^3P_1$, $^3P_2$, and $^1P_1$ states, respectively. Kang *et al*. have reported that the A and C bands appear at 3.7 and ~ 6.0 eV, respectively, in the absorption spectrum of KCl:Bi^{3+} at low temperatures [2].

In Bi^{3+} ions doped in fluoride hosts, the absorption bands would shift to the higher energy side, as compared to those in chloride hosts. In fact, in $CaF_2:Bi^{3+}$ and $SrF_2:Bi^{3+}$ crystals, the A band appears at ~ 5.8 eV and the C band at ~ 8.2 eV [3]. In $NaYF_4:Bi^{3+}$ crystals, the excitation band appearing at 5.0 eV is tentatively assigned as the A band nature due to $^1S_0 \rightarrow {}^3P_1$ transition in Bi^{3+} ions, although the transition energy is somewhat smaller compared with that of Bi^{3+} ions in other fluoride compounds. The excitation bands at 5.6 – 7.1 eV show composite structures, which is a common feature of the C band of Tl^+-type ions. Therefore, these structures in the VUV region is ascribed to the C band nature due to $^1S_0 \rightarrow {}^1P_1$ transitions in Bi^{3+} ions.

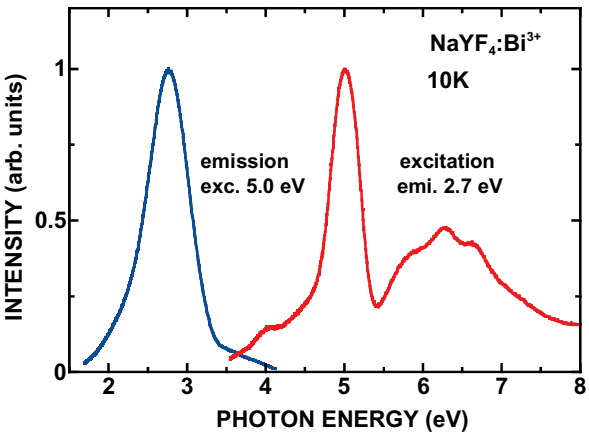

Fig. 1 Luminescence (blue curve) and excitation spectra (red curve) of $NaYF_3:Bi^{3+}$ at 10 K.

[1] W.B. Fowler, Physics of Color Centers, Academic Press Inc., New York, 1968.

[2] J.G. Kang, H.M. Yoon, G.M. Chun, Y.D. Kim and T. Tsuboi, J. Phys.: Condens. Matter **6** (1994) 2101.

[3] K.P. Oboth, F.J. Lohmeier and F. Fisher, phys. stat. sol. (b) **154** (1989) 789.

BL1B

Optical Anisotropy at the Absorption Edge in $CaMoO_4$ and $CaWO_4$

M. Fujita[1], M. Itoh[2], S. Takagi[2], T. Shimizu[2], N. Fujita[2]
[1]*Japan Coast Guard Academy, Wakaba, Kure 737-8512*
[2]*Department of Electrical and Electronic Engineering, Shinshu University, Nagano 380-8553*

Calcium tungstate is well known as intrinsic scintillation material. The crystal belongs to scheelite structure of tetragonal space group. The lowest absorption band of $CaWO_4$ was regarded as due to the transition to the 1*s* exciton state. Recent two-photon excitation experiment, however, suggests that the band is ascribed to the band-to-band transition [1].

In the present study, optical anisotropy of $CaMoO_4$ and $CaWO_4$ has been studied in order to clarify the nature of the lowest band as well as the structures at higher energy region.

Experiment

Single crystals of $CaMoO_4$ and $CaWO_4$ grown by the Czochralski method were used for the experiment. Reflectivity spectra were measured at 10 K for the polarization ***E*//*a*** and ***E*//*c*** using the polished surfaces of (010) plane. The optical constants such as dielectric functions were calculated from the reflectivity spectra using a Kramers-Kronig analysis.

Results and discussion

The solid curves in Fig. 1 show the spectra of imaginary part of dielectric functions (ε_2) of $CaMoO_4$ and $CaWO_4$ in the lowest band region. The broadness of these bands compared with the exciton band of $PbWO_4$ indicates that they are attributed to the band-to-band transition [1]. The width of the band for ***E*//*a*** is larger than that for ***E*//*c*** for both materials. In order to examine the band shape in detail, the spectra of the second-energy-derivative of ε_2 ($d^2\varepsilon_2/dE^2$) were calculated. The derivative spectra shown by the dotted curves in Fig. 1 indicate that the band consists of two components for ***E*//*a*** and a single component for ***E*//*c*** for both materials. Figure 2 shows the energy diagram of a MoO_4^{2-} (WO_4^{2-}) oxyanion molecule. In a free molecule of T_d symmetry, the highest occupied orbital is of t_1 symmetry of O2*p* character, and the lowest unoccupied orbital is of *e* symmetry of mainly Mo4*d* (W5*d)* character. In the scheelite crystal, the symmetry of the molecule is lowered to D_{2d} and both the t_1 and *e* orbitals split into two sublevels. The dichroism of the band in Fig. 1 can be explained well in terms of the assignment given in Fig. 2. Thus the optical excitation at the absorption edge in $CaMoO_4$ and $CaWO_4$ can be ascribed to the transition from the valence band of t_1 orbital to the conduction band made of *e* orbital in the oxyanion molecule.

Figure 3 shows the ε_2 spectra up to 30 eV. A clear correspondence between the structures in $CaMoO_4$ and $CaWO_4$ is seen with respect to the spectral shape and polarization dependence, as numbered in Fig. 3. The structures 2-4 are assigned to the transition from the valence band to the next higher conduction band of t_2 orbital of mainly Mo4*d* (W5*d)* character, and the structures 5-8 to the transition to the conduction band of the Ca state.

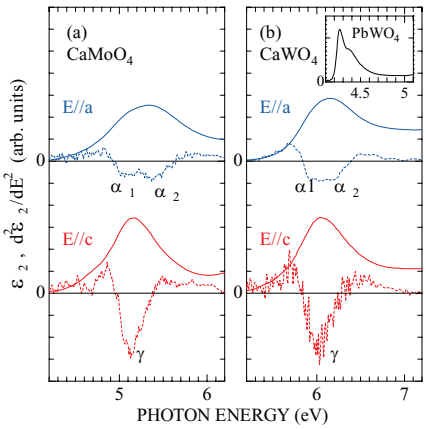

Fig. 1 The spectra of ε_2 (solid curves) and $d^2\varepsilon_2/dE^2$ (dotted curves) of (a) $CaMoO_4$ and (b) $CaWO_4$. The ε_2 spectrum of $PbWO_4$ [2] is shown in the inset of (b).

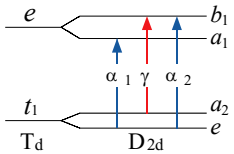

Fig. 2 Energy diagram of a MoO_4^{2-} (WO_4^{2-}) molecule of T_d and D_{2d} symmetry. Blue and red arrows indicate the allowed transitions for ***E*//*a*** and ***E*//*c***, respectively.

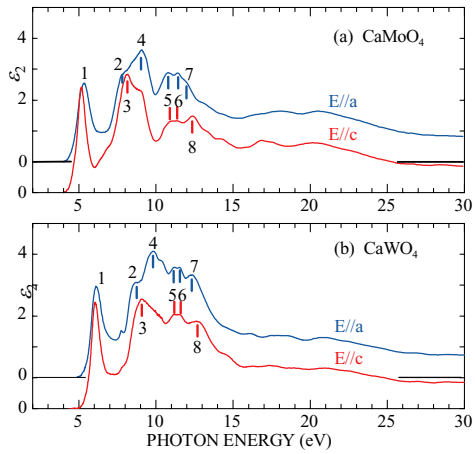

Fig. 3 The spectra of ε_2 of (a) $CaMoO_4$ and (b) $CaWO_4$ up to 30 eV.

[1] V. B. Mikhailik *et al.*, Phys. Rev. B **69** (2004) 205110.
[2] M. Fujita *et al.*, Phys. Rev. B **65** (2002) 195105.

BL1B

Photoluminescence in Polyamide-6/Mica Nanocomposite

N. Fuse[1], M. Okada[1], T. Tanaka[2], Y. Ohki[1]
[1]*Department of EEBS, Waseda University, Shinjuku 169-8555 Japan*
[2]*Graduate School of IPS, Waseda University, Kita-Kyushu 808-0135 Japan*

Dielectric properties of polymer nanocomposites (NCs) have been reported actively in recent years because of their wide potential application fields [1]. The present article reports photoluminescence (PL) and PL decay characteristics of polyamide-6, focusing on the effect of addition of mica nanofillers.

Experimental

The samples investigated are three kinds of polyamide-6 NCs with 2, 4 and 5 wt% addition of mica nanofillers. Mica was exfoliated to 1 nm thick layers, which were then uniformly dispersed in polyamide-6 resin by *in situ* polymerization [2]. As a reference, polyamide-6 without mica nanofillers was also used. The samples are called PA-0, PA-2, PA-4 and PA-5 according to their mica contents. Using synchrotron radiation (SR) under multi-bunch operation at the BL1B line of UVSOR Facility (Institute of Molecular Science, Okazaki, Japan, beam energy: 750 MeV) as a photon source, PL spectra from the samples were measured. The PL decay profiles were measured by a single photon counting method using SR under single-bunch operation (SR duration: 0.55 ns, interval: 176 ns). All the measurements were done at room temperature.

Results and Discussion

Fig. 1 shows a two-dimensional map that shows the PL intensity distribution observed for PA-0 by changing the excitation photon energy. The PL intensity is normalized by the maximum intensity of PL A that has an excitation peak around 3.6 eV and an emission peak around 3.0 eV. Another PL called PL B, which has an excitation peak around 4.8 eV and an emission peak around 2.9 eV, is also observed. Note that Band 1 is the excitation light, and that Band 2 is a fake replica of Band 1 that goes through the monochromator at the wavelength twice the designated value. Moreover, Bands 3 and 4 are originated from interference for the excitation light with the monochromator gratings. Therefore, only PLs A and B are the true PL spectra related to the samples.

Fig. 2 shows decay profiles of PLs A and B. For both PLs A and B, no change in the decay profile was induced by the addition of nanofillers. Namely, it is confirmed that the same two PLs, A and B, appear in all the samples irrelevantly to the nanofiller loading.

Further results show that neither the emission energies nor excitation energies of two PL bands change by the addition of nanofillers. Moreover, no new PLs are induced in the range from 2.0 eV to 6.0 eV. These are negative results for the appearance of new localized states in the forbidden band at least as long as luminous ones, while it has been reported that shallow traps are introduced in the forbidden band by the addition of nanofillers [3].

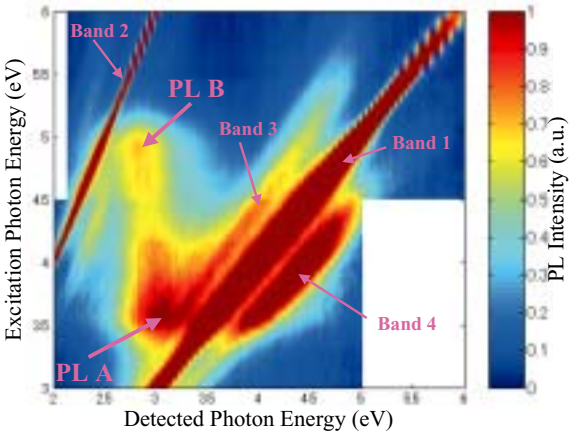

Fig. 1 Two-dimensional distribution of PL intensity induced by SR photons in PA-0.

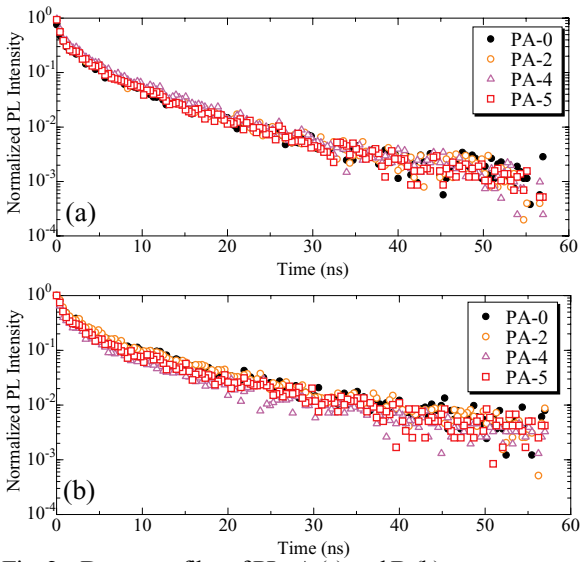

Fig. 2 Decay profiles of PLs A (a) and B (b).

[1] T. Tanaka *et al.*, IEEE Trans. Dielectr. Electr. Insul. **11** (2004) 763.
[2] S. Katahira *et al.*, Kobunshi Ronbunshu **55** (1998) 83 [in Japanese].
[3] G.C. Montanari *et al.*, IEEE Trans. Dielectr. Electr. Insul. **11** (2004) 754.

BL1B

Temperature Dependence of Absorption and Luminescence Spectra of $BaMgF_4:Ce^{3+}$ Crystals

E. Hayashi[1], Y. Ohsumi[1], T. Hasegawa[1], M. Yoshida[1], M. Yamaga[1], S. Ono[2], N. Sarukura[2]

[1]*Department of Electric and Electronic Engineering, Gifu University, Gifu 501-1193, Japan*

[2]*Institute for Molecular Science, Okazaki 444-8585, Japan*

Recently, laser materials operating in the vacuum ultraviolet (VUV) region below 200 nm is required. In order to satisfy this requirement, a frequency doubling method using a nonlinear effect is useful. Ce^{3+}-doped $BaMgF_4$ (BMF) crystals attract attention as laser materials with a nonlinear effect. In this report, we discuss temperature dependence of absorption and luminescence spectra of Ce^{3+} in BMF.

Figure 1 shows temperature dependence of absorption spectra of BMF:Ce^{3+}. The absorption spectra consist of four intense VUV bands at 115, 127, 144, and 157 nm, and five VUV/UV bands at 174, 199, 232, 246, and 258 nm. The latter is assigned as optical transitions from the $^2F_{5/2}$ ground state to five non-degenerated 5d excited states of Ce^{3+}. Shapes of three bands around 250 nm do not change below 100 K. However, in increasing a temperature above 100 K, the widths are broadened and the peaks are shifted to longer wavelengths with an amount of about 2 nm. The intense VUV bands may be due to complexes composed of color centre (two electrons trapped at an F^- vacancy) and Ce^{3+} impurity [1,2].

Figure 2 shows temperature dependence of luminescence spectra with different excitation wavelengths. Three luminescence bands denoted by A, B, and C are shifted to longer wavelengths in alphabetical order. Broadening and peak-shift of the absorption bands occur with an increase of temperature as shown in Fig. 1. Taking account of these effects, intensities of A and C luminescence bands are independent of temperature except those of A and B bands with 196-nm and 156-nm excitation. The A-band luminescence is due to Ce^{3+} ions substituting for Ba^{2+} ions. The B-band luminescence is due to Ce^{3+} ions perturbed by charge compensators. The C-band luminescence is assigned to a complex composed of Ce^{3+} and color centre [1,2].

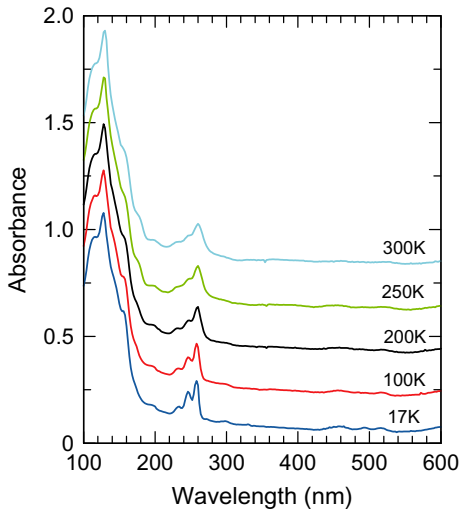

Fig. 1 Temperature dependence of absorption spectra of $BaMgF_4:Ce^{3+}$.

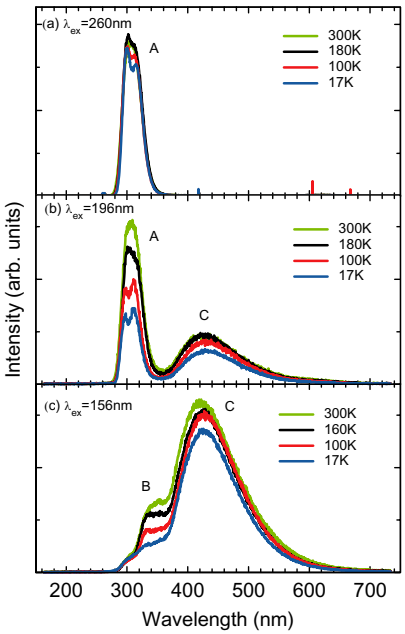

Fig. 2 Temperature dependence of luminescence spectra of $BaMgF_4:Ce^{3+}$.

[1] E. Hayashi, K. Itoh, S. Yabashi, M. Yamaga, N. Kodama, S. Ono and N. Sarukura, J. Alloys and Compounds **408-412** (2006) 883.

[2] E. Hayashi, K. Itoh, S. Yabashi, M. Yamaga, N. Kodama, S. Ono and N. Sarukura, J. Lumin. (2006) in press.

BL1B

Effect of Alkyl Chain Length on Photoionization at the Water Surface

T. Ishioka, A. Harata

Department of Molecular and Material Sciences, Kyushu University, Kasugakoen 6-1, Kasuga-shi, Fukuoka 816-8680, Japan

Photocurrent has been measured from anthra-quinone derivatives at the water surface by synchrotron radiation. Photoionization threshold did not change by elonging alkyl chains bound to the molecule but its intensity increased from C_2 to C_8 and then drastically decreased at C_{12}. It is suggested that solvation of anthraquinone by water is not largely influenced by alkyl chains but electrons emitted are remarkably scattered when alkyl chains are long enough to form self-assembled layers.

Introduction

Photoionization at the water surface give useful information on electric states and structures of adsorbed species and SR light has been used for measuring precise threshold energy by its inherent tunability in photon energy. However, photoionizing behavior of adsorbed molecules at an aqueous solution surface has not fully studied even though there are a wide variety of surface-active molecules and their adsorption behavior has a great importance in physical chemistry, biochemistry, environmental chemistry, and technology.

We have analyzed photoionizing behavior of dye molecules with surfactant layers over the adsorbed dye [1]. From the measurement, aggregation of dye molecules, self-assembled layer formation of surfactamts, and charge interactions between dye and surfactant molecules had a large effect on measured photoionization current. However, it was too difficult to distinguish each contribution from others because of complex surface constructions.

In this report, anthraquinone derivatives with alkyl chains were synthesized for simplifying the surface construction. Photoionization behavior on water surface is analyzed using this simple system and effects of alkyl chains are discussed.

Experimental

The monochromated synchrotron light (4-8 eV) was obtained from BL1B at the UVSOR facility and emitted from the chamber to a He-purged cell through an MgF_2 window. The emitted light was reflected on an Al mirror and vertically irradiated on the aqueous solution surface through a Cu-mesh electrode. The electrode was set at 5 mm high above the liquid surface and high voltage (400 V) was applied. The photocurrent (~100 fA) was measured by a picoammeter.

Anthraquinone derivatives modified with alkyl chains via thiourea (Fig. 1) were synthesized from 1-aminoanthraquinone and dissolved in benzene at 0.2 mM. The benzene solution was spread by 10 μL on the pure water surface.

Results and Discussion

In all cases, photoionization current increased above approximately the same threshold energies around 6.2 eV (Fig. 2). Since the threshold energy of molecule on the water surface is lowered by polarization energy of solvation, the difference of measured threshold from gas-phase ionization potential reflects the state of solvation. Unchaged threshold energy by elongation of alkyl chain length shows that the solvation state of water around anthraquinone ring is not largely distorted by the presence of hydrophobic functional groups.

However, photoionization intensity itself largely depends on the length of alkyl chains. For the shorter case, the small intensity can be explained by a loss of surface molecule to the bulk phase by its slight solubility to water. While C_{12} case, the decrease should arise from another reason. The observation of increased fluctuation of current at C_8 would suggest the presence of aggregated species on the surface. Thus it is considered that self-assembled layer is formed at C_{12} and electrons emitted are scattered by alkyl layers formed on the water surface.

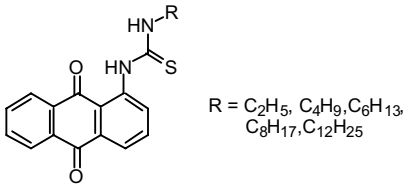

Fig. 1 Structure of synthesized anthraquinone derivatives.

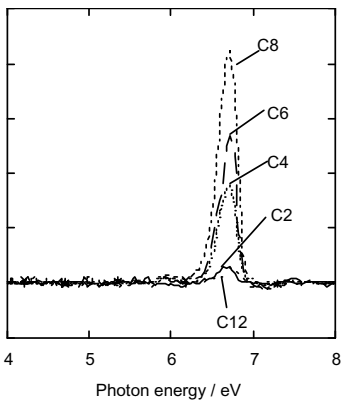

Fig. 2 Measured photoionization current from anthraquinone derivatives on the water surface.

[1] T. Ishioka and A. Harata, UVSOR Activity Report 2003 (2004) 62.

BL1B

Optical Properties of Tl^+ Centers Doped in CsH_2PO_4

T. Kawai[1], T. Hirai[2], N. Ohno[2,3]

[1]*Graduate School of Science, Osaka Prefecture University, Sakai 590-0035, Japan*

[2]*Academic Frontier Promotion Center, Osaka Electro-Communication University*

[3]*Graduate School of Engineering, Osaka Electro-Communication University, Neyagawa 572-8530, Japan*

Tl^+ centers doped in alkali halide crystals with the NaCl-type crystal structure exhibit three absorption bands called A, B and C in an energy region below the absorption edge of host crystals [1,2]. The absorption bands are attributed to the intraionic transitions corresponding to $^1S_0 \rightarrow {}^3P_1$ (spin-orbit allowed), $^1S_0 \rightarrow {}^3P_2$ (vibration induced), $^1S_0 \rightarrow {}^1P_1$ (dipole allowed), respectively. On the other hand, the Tl^+ centers doped in cesium halide crystals with the CsCl-type crystal structure exhibit remarkably different absorption bands from those doped in the NaCl-type alkali halides. Though the Tl^+ ions doped in NaCl- and CsCl-type alkali halide crystals are situated under the highest symmetry O_h, these ion arrangements around the Tl^+ ions are different in both the crystals. Optical properties of an impurity center are strongly affected by ion arrangements and the symmetry around the center. Therefore, it is of great interest to study the optical properties of the Tl^+ center doped in host crystals with lower symmetries.

In the present study, we have investigated optical properties of the Tl^+ center doped in CsH_2PO_4 (CDP), which belongs to a family of ferroelectric materials of the KH_2PO_4 (KDP) type. The crystal structures of KDP and CDP are orthorhombic and monoclinic at low temperature, respectively. Therefore, the Tl^+ ions doped in both crystal are situated under the lower symmetry. It is known that the Tl^+ center doped in KDP exhibits five characteristic polarized absorption bands [3,4]. On the other hand, there are few studies on optical properties of the Tl^+ center doped in CDP.

The CDP compound was synthesized by mixing stoichiometric amounts of Cs_2CO_3 and H_3PO_4. After several times of recystallization, TlH_2PO_4 (TDP) compound was added to the aqueous solution of the purified crystals. Crystals of CDP:Tl^+ were grown by an ordinary evaporation method from the CDP saturated aqueous solution doped with about 10^{-3} mol% TDP. Absorption, luminescence and excitation spectra of CDP:Tl^+ have been measured at the BL-1B beam line of UVSOR.

Figure 1 shows absorption (blue curve), luminescence (green curve), excitation (red curve) spectra of CDP:Tl^+ at 10 K. The absorption bands are observed at 5.86 and 7.54 eV. Their energy values are almost equal to those of the A and C absorption bands in KDP:Tl^+, respectively [3,4]. Therefore, the 5.86 and 7.54 eV bands in CDP:Tl^+ would be attributed to the A and C absorption bands.

When the A band at 5.86 eV is photo-excited, a broad luminescence band with a large Stokes shift is observed at 4.13 eV. The 4.13 eV luminescence band exhibits non-Gaussian bandshape and the lower energy tail. The fact implies that the 4.13 eV band is composed of several luminescence bands. The excitation spectrum for the 4.13 eV band exhibits the strong response on 5.86 eV light. The fact indicates that the 4.13 eV band is related with the Tl^+ center doped in CDP. Since there is a response on the lowest A absorption band in the excitation spectrum, the 4.13 eV luminescence band should be ascribed to a radiative transition from the relaxed excited states of $^3P_1$.

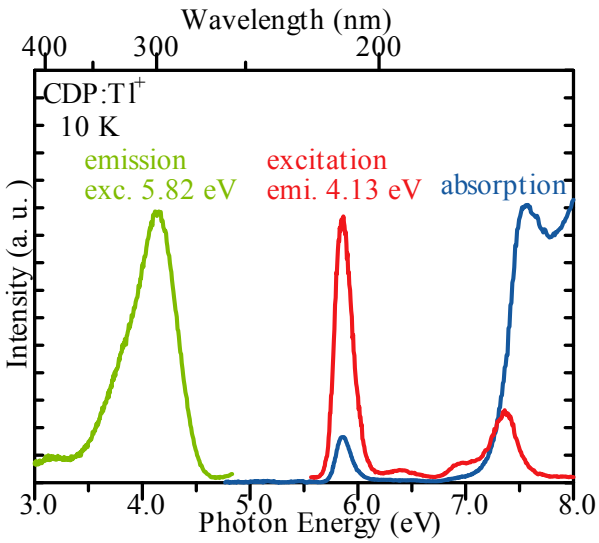

Fig. 1 Absorption (blue curve) and luminescence (green curve) and excitation (red curve) spectra of CDP:Tl^+ at 10K.

[1] A. Ranfagni *et al*., Adv. Phys. **32** (1983) 8253.
[2] P.W.M. Jacobs, J. Phys. Chem. Solids **52** (1991) 35.
[3] I. Fujita, Phys. Rev. B **49** (1994) 6462.
[4] T. Fuyuki and N. Ohno, UVSOR Activity Report 2004 (2005) 69.

BL1B

Vacuum-Ultraviolet Reflectance Spectroscopy of 3d Transition-Metal Oxides

I. Kezsmarki[1], S. Miyasaka[1] Y. Tomioka[2], Y. Tokura[1,2,3]

[1]*Department of Applied Physics, University of Tokyo, Tokyo 113-8656 Japan*

[2]*Correleted Electron Research Center (CERC), National Institute of Advanced Industrial Science and Technology (AIST), Tsukuba 305-8562 Japan*

[3]*Spin Superstructure Project (SSS), ERATO, Japan Science and Technology Agency (JST), Tsukuba 305-8562 Japan*

One of the most important characteristics for the strongly correlated electron systems is the drastic re-construction of electronic structure over an energy scale of eV with changes of temperature, doping concentration and so on. In this beam time, we measured the reflectivity spectra for single crystals of perovskite-type $R_{1-x}A_xMnO_3$ (R=trivalent rare-earth elements, A=divalent alkaline-earth ones) with the hole concentration of x=0.45, for an energy range of 4 eV < E < 35 eV using the beam line BL1B. The measured reflectivity data, together with that below 4 eV, were used to derive the optical conductivity spectra via the Kramers-Kronig analysis.

It is well known that the magnetic and electronic characters are controlled by the doping concentration and the effective one electron band-width in $R_{1-x}A_xMnO_3$. Recent studies have indicated that the bicritical feature caused by the competition between the ferromagnetic metal (FM) and charge/orbital ordering (CO/OO) insulator plays an important role in the colossal magnetoresistance effect. In addition, it has been revealed that the effect of quenched disorder due to the random chemical replacement of the perovskite A site is one of controllable parameters [1]. In $R_{0.55}Sr_{0.45}MnO_3$, the transition temperature of the ferromagnetic ordering (T_C) decreases from ~ 280 K to ~ 50 K, as R changes from Nd to Eu, i.e., as the effective one electron band-width decreases. In R=Gd compound, the ferromagnetic state becomes further unstable, and then the FM is taken over by a spin glass-like insulator below T_G= ~ 50 K. In the $Pr_{0.55}(Ca_{1-y}Sr_y)_{0.45}MnO_3$ system, by contrast, the reduction in T_C is not so remarkable as in the $R_{0.55}Sr_{0.45}MnO_3$ system. Moreover, the phase change from a FM to a CO/OO (long range) insulator is typically bicritical with T_C=T_{CO} ~ 200 K. That is, the phase diagram of the $R_{0.55}Sr_{0.45}MnO_3$ system is different from the bicritical feature in spite of the common hole-doping level and even when the average radius of the perovskite A site is taken as the same value. The dramatic modification of the FM vs CO/OO phase diagrams is quite analogous to the case of the A-site order versus disorder of $R_{0.5}Ba_{0.5}MnO_3$, where the perfect R/Ba ordering along the c axis alters the phase diagram of the R/Ba solid solution (similar to that of the R/Sr solid solution) to the typical bicritical phase diagram (similar to that of $Pr_{0.55}(Ca_{1-y}Sr_y)_{0.45}MnO_3$) [2]. Therefore, the large modification of the phase diagram in $R_{0.55}Sr_{0.45}MnO_3$ case is likely to arise from the random potential affecting on the FM vs CO/OO bicritical feature. The source of the random potential may be the local lattice distortion arising from the larger mismatch of the ionic size of R/Sr ions than Pr/(Ca, Sr) ones.

We present the optical conductivity spectra for $R_{0.55}Sr_{0.45}MnO_3$ (R=Nd and Eu) in Fig. 1. In the spectra at high temperatures, the lowest optical transition around 1 eV can be assigned to the optical transition across the Mott-type gap. Above the Mott gap, a much more intense optical transition is clearly discerned. The position and intensity suggest that the transition be assigned to the charge transfer excitation from O 2p to Mn 3d upper Hubbard state. In the temperature region of T<T_C, the Mott gap disappears and the spectral weight around 1 eV is transferred to the lower energy region. Resultantly, the Drude-like structure appears below T_C. The spectral change takes place at about room temperature in $Nd_{0.55}Sr_{0.45}MnO_3$, while that occurs below 50 K in $Eu_{0.55}Sr_{0.45}MnO_3$.

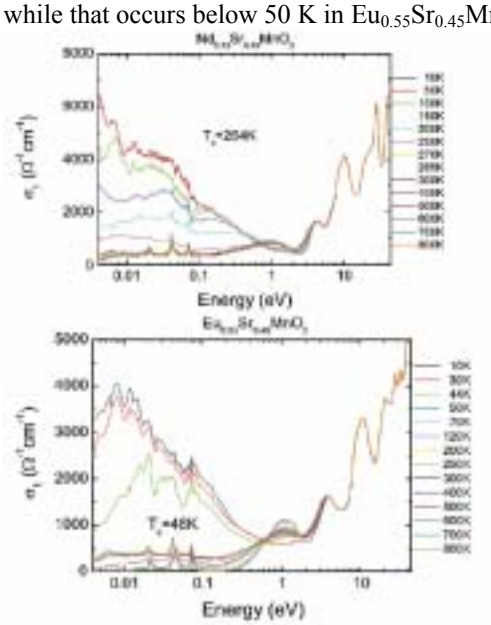

Fig. 1 The optical conductivity spectra (σ_1) for $R_{0.55}Sr_{0.45}MnO_3$ (R=Nd and Eu) at various temperatures.

[1] Y. Tomioka *et al.*, Phys. Rev. B **68** (2005) 094417.
[2] D. Akahoshi *et al.*, Phys. Rev. Lett. **90** (2003) 177203.

BL1B

Photoluminescence of Hydroxyapatite Irradiated by Ultraviolet Synchrotron Orbital Radiation Light (2)

M. Ohta

Department of Material Science and Technology, Faculty of Engineering, Niigata University, 8050 Ikarashi 2-no-cho, Niigata 950-2181, Japan

It was known that rare earth ions dosed for oral administration to mouse and rat are transferred to blood vessel through the ileum and deposited its teeth and bone, which mainly consists of hydroxyapatite (HAp; $Ca_{10}(PO_4)_6(OH)_2$) [1-2]. We have found that Eu ion substituted Ba ion in Eu doped $Ba_{10}(PO_4)_6Cl_2$ phosphor, which matrix is apatite structure [3]. In this study, rare earth ion-doped HAp samples were prepared in order to make clear the segregation mechanism of rare earth ion on teeth and bone. Their characteristics were investigated by photoluminescent (PL) property of rare earth ion-doped HAp excited by ultraviolet synchrotron orbital radiation light.

Eu-doped HAp and Gd-doped HAp were prepared as follows: HAp was soaked at 310K in $EuCl_3$ or $GdCl_3$ aqueous solution. After 72 hr, Eu-doped or Gd-doped HAp was separated from $EuCl_3$ or $GdCl_3$ aqueous solution by filtation and then dried by using with infrared ray (unfired samples). Fired samples were prepared by firing the unfired samples at 1373K for 1 hr in air.

The PL property of each sample exited by ultraviolet synchrotron orbital radiation light (BL1B) was detected by using with a multi-channel analyzer.

Figure 1 shows PL spectra of unfied and fired Eu-doped HAp samples excited by BL1B. The PL spectra of both Eu-doped HAp samples exited by 120 nm or 160 nm had many peaks which were not ascribed to Eu ion. These facts indicate the inner shell excitation in host crystals and traps of electron and/or hole due to the defects of host crystal structure exits in both Eu-doped HAp samples, since the PL property is similar to that of self doped phosphors. The PL spectra of both Eu-doped HAp samples exited by 200 nm or 240 nm had the peaks due to the f-f electronic transitions of trivalent Eu ion as from $^5D_0$ to $^7F_1$ (595 nm), from $^5D_0$ to $^7F_2$ (612 nm), from $^5D_0$ to $^7F_3$ (654 nm) and from $^5D_0$ to $^7F_6$ (700 nm). These PL peaks height of fired sample was higher than that of unfired sample.

Figure 2 shows PL spectra of unfired and fired Gd-doped HAp samples excited by BL1B. The PL spectra of unfired Gd-doped HAp sample had many peaks which were not ascribed to Gd ion, even if exited by 120-240nm. While the PL spectra of fired Gd-doped HAp sample exited by 120-240nm had the peaks due to the f-f electronic transition of trivalent Gd ion as from $^6P_{7/2}$ to ^8S (316 nm), especially, the peak height of the sample exited by 160 nm was remarkably large.

These facts indicate that Eu and Gd ions deposit in the surface of HAp and Eu ion substitute for Ca ion in HAp according to ion exchange reaction at 310K. The fired samples are higher crystallinity and exhibit brighter PL due to the f-f-electronic transition of trivalent Eu and Gd ion.

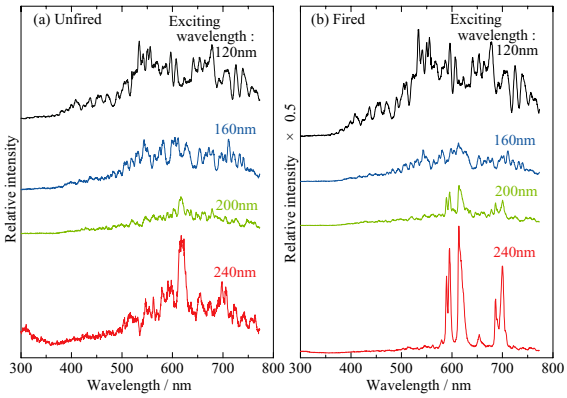

Fig. 1 Photoluminescence spactra of Eu-doped HAp sample excited by ultraviolet synchrotron orbital radiation light.

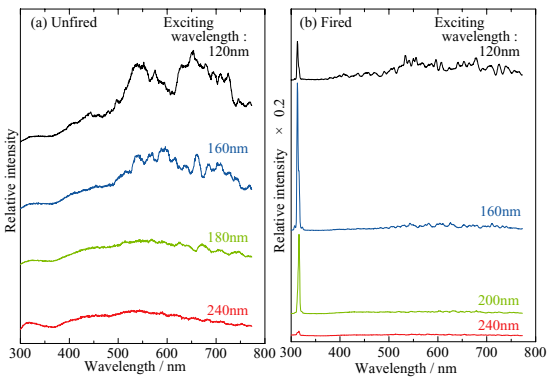

Fig. 2 Photoluminescence spactra of Gd-doped HAp sample excited by ultraviolet synchrotron orbital radiation light.

[1] S. Hirano, K. T. Suzuki, Environ. Health Perspect. **104** (Supplement 1) (1996) 85.
[2] K. Kostial, B. Kargacin, M. Lendeka, Int. J. Radiat. Biol. Relat. Stud. Phys. Chem. Med. **51** (1987) 139.
[3] M. Sato, T. Tanaka, M. Ohta, J. Electrochem. Soc., **141** (1994) 1851.

BL1B

Photoluminescence from Langasite $La_3Ga_5SiO_{14}$ Crystals

S. Takagi[1], T. Shimizu[1], M. Itoh[1], M. Fujita[2], M. Kitaura[3]
[1]*Faculty of Engineering, Shinshu University, Wakasato, Nagano 380-8553*
[2]*Japan Coast Guard Academy, Wakaba, Kure 737-8512*
[3]*Fukui National College of Technology, Sabae 916-8507*

Lanthanum gallium silicate (langasite; $La_3Ga_5SiO_{14}$) is a new piezoelectric crystal and is abbreviated to LGS. The absence of structural phase transitions between the melting point (1470°C) and room temperature makes the application of this material at elevated temperatures feasible [1]. The crystal of LGS consists of tetrahedral layers, perpendicular to the crystalline *c*-axis, between which there are layers formed by cations in distorted cubes coordinated by eight O atoms and in octahedral by six O atoms.

Because of the strong exciton-phonon interaction in LGS, it is very interesting to investigate whether a self-trapped exciton (STE) exists or not. Bearing this in mind, we performed luminescence measurements of LGS at low temperatures.

Experiment

The single crystals of LGS used in this work were obtained from Mitsubishi Materials, Japan. They were grown by the Czochralski method, and annealed at 1000–1300°C for 24 h in reduced atmosphere. Three-dimensional (3-D) emission-excitation spectra were measured using an Acton SpectraPro-3000i monochromator equipped with an LN/CCD camera.

Results and Discussion

Figure 1 shows the 3-D spectrum of LGS measured at 5 K under the condition that the electric vector of the incident light is parallel to the *Y*-axis of a sample. The lower part corresponds to the contour plot of the upper spectrum. One may see two emission bands at 420 and 500 nm. The intensity of the 420 nm band increases at 220 nm, and reaches the maximum around 205 nm, followed by the decrease in the short wavelength region. The 500 nm band is strongly excited with UV light at around 245 nm. The 3-D spectrum for the polarization parallel to the *Z*-axis was almost the same as Fig. 1, indicating that there is no appreciable polarization characteristic of two emission bands at 420 and 500 nm.

The electronic structure of LGS has been studied experimentally and theoretically [2]. The valence band is mainly formed by the O 2*p* states, and the lower part of the conduction band is dominated by the La 5*d* states. The excitation threshold of the 420 nm band coincides with the fundamental absorption edge at ≈ 235 nm. Such a coincidence suggests that this band is of intrinsic origin. It is likely that a hole is self-trapped at an oxygen ion because of the strong coupling with phonons. As a result, an STE is formed through the capture of a conduction electron by the self-trapped hole. We suppose that the 420 nm band is ascribed to the radiative annihilation of STEs. On the other hand, the 500 nm band is due to the decay of localized excitons perturbed by some lattice imperfection, because it is induced in the energy region below the fundamental absorption edge.

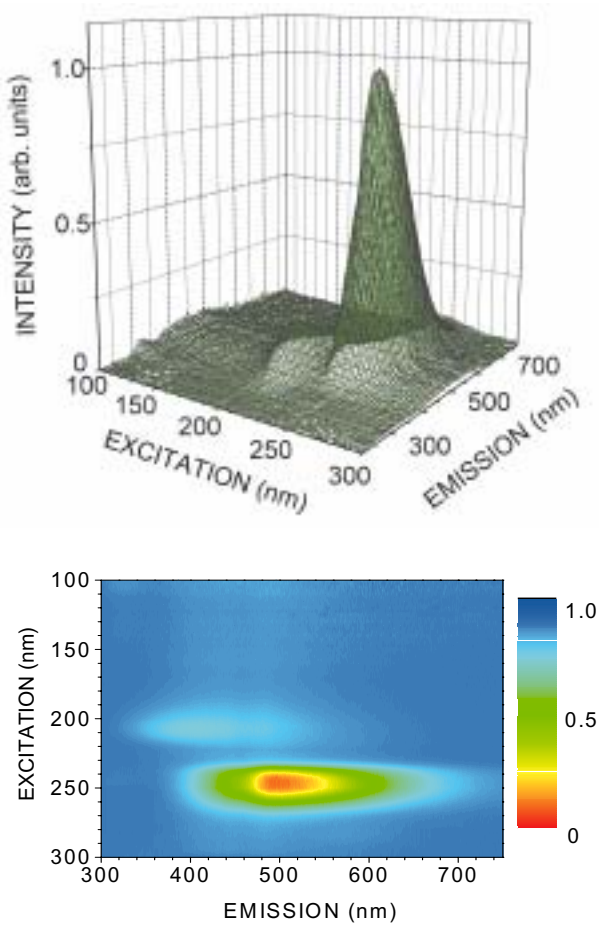

Fig. 1 3-D emission-excitation spectrum of LGS measured for the polarization parallel to the *Y*-axis, together with the contour plot of the upper spectrum.

[1] K. Shimamura, H. Takeda, T. Kohno and T. Fukuda, J. Cryst. Growth **163** (1996) 388.
[2] M. Kitaura, K. Mochizuki, Y. Inabe, M. Itoh, H. Nakagawa and S. Oishi, Phys. Rev. B **69** (2004) 115120.

BL1B

Luminescence Properties of $YAl_3(BO_3)_4$ Substituted with Sc^{3+} Ions

H. Yoshida[1,2], K. Fujikawa[1], H. Toyoshima[1], S. Watanabe[1], K. Ogasawara[1]

[1]*Department of Chemistry, Kwansei Gakuin University, 2-1 Gakuen, Sanda, 669-1337, Japan*

[2]*Research and Development Division, NEC Lighting, Ltd., 3-1 Nichiden, Minakuchi-cho, Koka, 528-8501, Japan*

Introduction

The $YAl_3(BO_3)_4:Gd^{3+}$ (YAB:Gd) phosphor has a strong ultraviolet (UV) emission line at 3.96 eV, which is effectively stimulated under the vacuum ultraviolet excitation. Its crystal structure (space group *R*32) is isostructural with the mineral huntite, $CaMg_3(CO_3)_4$. One of the interesting points is that there are two kinds of BO_3 atomic groups within an unit cell of $YAl_3(BO_3)_4$ (YAB) crystal. Recently, we successfully explained the origin of the excitation spectrum of YAB:Gd phosphor by the first-principles method [1]. Moreover, as we expected, it was confirmed that the luminescence peak intensity of $Y_{0.65}Gd_{0.25}Sc_{0.1}Al_3(BO_3)_4$ was about 1.4 times that of YAB:Gd phosphor [2]. However, the mechanisms of the excitation processes with the presence of Sc^{3+} ions are not fully understood. To clarify the origin of this luminescence enhancement, luminescence and excitation spectra of YAB and $Y_{0.9}Sc_{0.1}Al_3(BO_3)_4$ (YSAB) have been measured at low temperature.

Sample Preparation Method

YAB and YSAB samples were synthesized with a solid-state reaction using Y_2O_3 (4N), H_3BO_3(2N) Al_2O_3(5N) and Sc_2O_3(3N) as the starting materials. The powder samples were obtained by firing in air for 20 hours at 1450 K.

Results and Discussion

Yokosawa *et al.* reported that UV emission band at about 310 nm is obserbed for YAB under VUV excitatuon [3]. Figure 1 shows the excitation spectra of YAB and YSAB detected at the emisson peak position. In the YAB, the valence band of our calculations is mainly build of O 2*p* state and the conduction band is composed of mixing state of the B 2*p* and Y 4*d* [1]. Therefore, a clear structure peaking at 7.8eV corresponds to transitions from O 2*p* state to the mixed state of B 2*p* and Y 4*d*. As we can see, the absorption edge of YSAB is lower energy side than that of YAB. It is concluded that the origin of additional structure at about 7 eV is due to the Sc 3*d* states according to the electronic state calculation by DV-Xα method.

In fig. 2, the luminescence spectra of YAB and YSAB are shown. As we can see, it is found that these emission peek position were different. In YAB, two emission bands peaking at 3.2 and 3.9 eV are observed. On the other hand, there appear two emission bands at 3.2 and 4.1 eV in YSAB. The origins of these emission bands are ascribed to BO_3 atomic groups [3], and we suppose that the shift of the peak around 3.9-eV emission bands is deeply related to the fact that one kind of BO_3 atomic groups of YSAB are significantly distorted compared to that of YAB. It is still a question as to how 3.9-eV band shifts toward higher energy side by Sc^{3+} substitution. The obtained results suggested the need for further experiments and theoretical considerations.

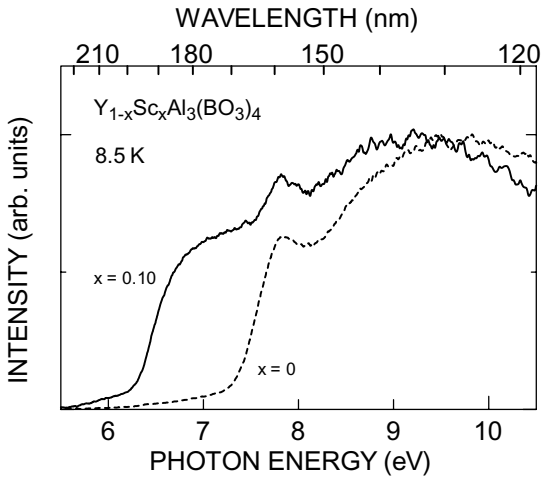

Fig. 1 Excitation spectra of $YAl_3(BO_3)_4$ (solid line) and $Y_{0.9}Sc_{0.1}Al_3(BO_3)_4$ (dash line) at 8.5 K.

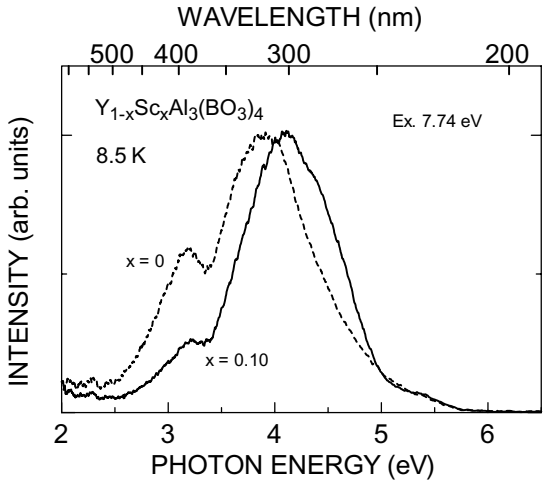

Fig. 2 Luminescence spectra of $YAl_3(BO_3)_4$ (solid line) and $Y_{0.9}Sc_{0.1}Al_3(BO_3)_4$ (dash line) at 8.5 K.

[1] H. Yoshida, R. Yoshimatsu, S. Watanabe and K. Ogasawara, Jpn. J. Appl. Phys. **45** (2006) 146.

[2] H. Yoshida, R. Yoshimatsu and K. Ogasawara, J. Lumin. to be published.

[3] N. Yokosawa and E. Nakazawa, Jpn. J. Appl. Phys. **42** (2003) 5656.

BL1B

Luminescence Properties of $(Y,Gd)Al_3(BO_3)_4:Tb^{3+}$ Phosphors Substituted with Sc^{3+} Ions

H. Yoshida[1,2], K. Fujikawa[1], H. Toyoshima[1], S. Watanabe[1], K. Ogasawara[1]

[1]*Department of Chemistry, Kwansei Gakuin University, 2-1 Gakuen, Sanda, 669-1337, Japan*

[2]*Research and Development Division, NEC Lighting, Ltd., 3-1 Nichiden, Minakuchi-cho, Koka, 528-8501, Japan*

Introduction

Plasma display panels (PDPs) and new mercury-free lamps using xenon discharge have been developed and required new phosphors with high efficiency. Especially, a green phosphor is deeply related to the luminous intensity. Tanimizu *et al.* [1] and Yokosawa *et al.* [2] reported that the efficiency of luminescence for Tb^{3+} activated $YAl_3(BO_3)_4$ phosphor under vacuum ultraviolet (VUV) excitation is almost the same as that of Zn_2SiO_4:Mn which is a green phosphor of typical PDPs. However, the efficiency is not enough and more improvement of luminescence properties are demanded. Recently, we reported the luminescence properties of $YAl_3(BO_3)_4$:Gd substituted with Sc^{3+} ions that has a higher efficiency of luminescence than that of $YAl_3(BO_3)_4$:Gd. In this study, we have been investigated the luminescence and excitation spectra of $(Y,Gd)Al_3(BO_3)_4:Tb^{3+}$ phosphors substituted with Sc^{3+} ions at low temperature.

Results and Discussion

Figure 1 shows the luminescence spectrum of $Y_{0.55}Gd_{0.25}Tb_{0.2}Al_3(BO_3)_4$ phosphor under the excitation light at 7.74 eV. As we can see, the several strong emission lines are observed. The 2.29-eV emission line is useful as a green emission, which orginates from the $^5D_4 \rightarrow {}^7F_5$ transitions in Tb^{3+} ions. In Fig. 2, excitation spectra of $Y_{0.55-x}Gd_{0.25}Tb_{0.2}Sc_xAl_3(BO_3)_4$ (x = 0, 0.05, 0.10, 0.15, 0.20, 0.25) detected at 2.29-eV emission line are shown. A clear structure peaking at 7.8 eV corresponding to transitions from O 2*p* state to mixture state of B 2*p* and Y 4*d* orbitals [3]. The structure in the range from about 4.5 eV to 7 eV is assigned to $4f^9$-$4f^8 5d^1$ transitions in Tb^{3+} ions. It is clearly found that the intensity of excitation band at about 6.8 eV increases with increasing Sc concentration. We suppose that this additional excitation band is due to the Sc 3*d* state, which is a good agreement with our calculation results of the electronic state by the first principles DV-Xα method [4]. We have also confirmed that the luminescence peak intensity and luminance of $Y_{0.55-x}Gd_{0.25}Tb_{0.2}Sc_xAl_3(BO_3)_4$ (x = 0.10) at room temperature is stronger by a factor of about 1.3 compared with $Y_{0.55}Gd_{0.25}Tb_{0.2}Al_3(BO_3)_4$ under the VUV excitation light (peak wavelength:172 nm) using a xenon excimer lamp.

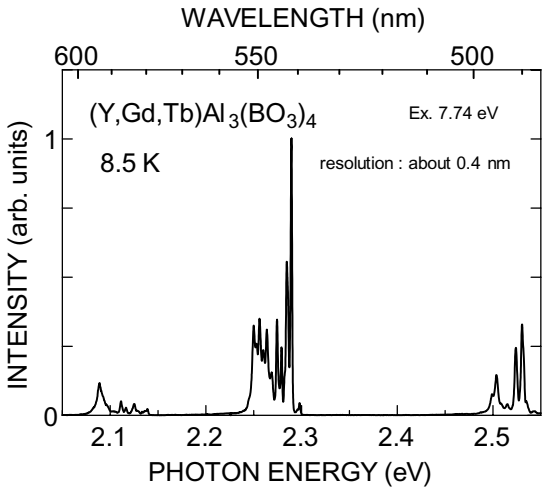

Fig. 1 Luminescence spectrum of $Y_{0.55}Gd_{0.25}Tb_{0.2}Al_3(BO_3)_4$ at 8.5 K.

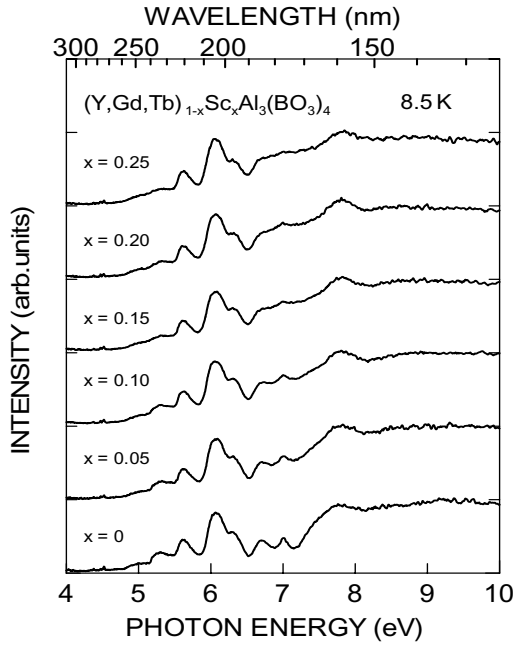

Fig. 2 Excitation spectra of $Y_{0.55-x}Gd_{0.25}Tb_{0.2}Sc_xAl_3(BO_3)_4$(x = 0, 0.05, 0.10, 0.15, 0.20, 0.25) at 8.5 K.

[1] S. Tanimizu, T. Suzuki, M. Shiiki and C. Okazaki, Proc. 9th Int. Symp. Sci. Tec. Light Sci. (2001) 393.
[2] N. Yokosawa, K. Suzuki and E. Nakazawa, Jpn. J. Appl. Phys. **42** (2003) 5656.
[3] H. Yoshida, R. Yoshimatsu, S. Watanabe and K. Ogasawara, Jpn. J. Appl. Phys. **45** (2006) 146.
[4] H. Yoshida, R. Yoshimatsu and K. Ogasawara, J. Lumin. to be published.

BL5B

Photoinduced Change in Vacuum Ultraviolet Transmission Spectra of Amorphous Chalcogenide Films Induced by Bandgap Light

K. Hayashi

Department of Electrical and Electronic Engineering, Gifu University, Gifu 501-1193, Japan

Introduction

It is well known that amorphous chalcogenide semiconductor materials, such as amorphous As_2S_3 (a-As_2S_3) and amorphous As_2Se_3 (a-As_2Se_3), show a variety of photoinduced phenomena [1-3]. The most prominent photoinduced phenomenon is the so-called photodarkening arising from the shift of the absorption edge. The absorption edge shifts to lower energy side by irradiation of light with the energy corresponding to the optical bandgap. For well annealed sample, the darkened state is removed by annealing near the glass-transition temperature. The X-ray diffraction and the volume change before and after irradiation suggest that the photodarkening is due to a change of local structure of the amorphous network [2]. Although a large number of studies have been done on the photodarkening induced by irradiation of bandgap (BG) light, the details of the mechanism is still unknown. To our knowledge, little attention has been given to the change of other energy structure induced by irradiation of BG light. To obtain a wide knowledge of the photoinduced phenomena, it is necessary to investigate photoinduced phenomena over a wide energy range. In previous reports, we reported photoinduced change in spectra of the vacuum ultraviolet (VUV) reflection and the total photoelectric yield by irradiation of BG light [4]. In this report, we investigate photoinduced change in VUV transmission spectra of amorphous chalcogenide films induced by irradiation of BG light.

Experimental

Thin films of amorphous chalcogenide semiconductor (a-As_2S_3 and a-As_2Se_3) were prepared onto ultrathin collodion films by conventional evaporation technique. A typical thickness of an amorphous film was around 160 nm. The ultrathin collodion films were prepared onto stainless steel metal plates in which two pinholes of the 1.5 mm diameter opened. A xenon arc lamp with IR-cut-off filter was used as a BG light source. Before the measurement of the VUV transmission spectrum, the unilateral of the sample was irradiated with the BG light in a vacuum to the degree in which the sample sufficiently produced the photodarkening. The measurement of the VUV transmission spectra were carried out at room temperature at the BL5B beam line of the UVSOR facility of the Institute for Molecular Science. And the spectrum was measured by using the silicon photodiode as a detector. To eliminate the higher order light from the monochromator, an aluminum thin film was inserted between the monochromator and sample. We also monitored the spectrum of the light source by measuring the photoelectric yield of a gold mesh.

Results and Discussion

Figure 1 shows the VUV transmission spectra of a-As_2S_3 film at room temperature in the photon energy region between 41 and 49 eV. One main absorption peak was observed in this energy region. This absorption peak around 44 eV corresponds to the 3d core level of As atom. As shown in Fig. 1, after irradiation with BG light, the absorption peak slightly shifts to higher energy side and the width of the spectrum becomes narrow. The similar change is also observed in the VUV reflection spectrum and a-As_2Se_3 films. As for the origins of the changes, it is not clear. I think that these changes are related to a change of the local structure of the amorphous network by irradiation of BG light. The detailed experiments and analysis will be done in the next step.

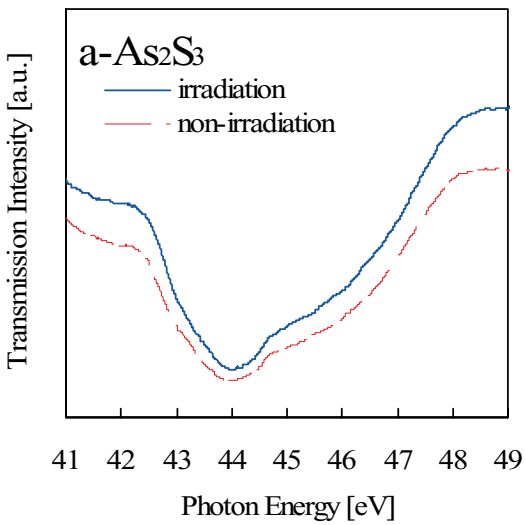

Fig. 1 The VUV transmission spectra of a-As_2S_3 film in non-irradiation part (broken line) and irradiation part (solid line) of BG light.

[1] Ke. Tanaka, Rev. Solid State Sci. **4** (1990) 641.
[2] K. Shimakawa, A.Kolobov, and S. R. Elliott, Adv. Phys. **44** (1995) 475.
[3] Ke. Tanaka, Encyclopedia of Nanoscience and Nanotechnology **7** (2004) 629.
[4] K. Hayashi, UVSOR Activity Report 2001 (2002) 126.

BL6B(IR)

Electronic Structure Analysis of Pt Clusters with Far-IR

Y.-T. Kim, K. Ohshima, A. Fujiwara, T. Mitani
School of Materials Science, Japan Advanced Institute of Science and Technology, Ishikawa 923-1292 Japan

It is well-known that the band structure for bulk materials is changed into the discrete electronic structure with size decreasing. This phenomenon can be understood with a quantum size effect (QSE) due to the confined electronic wave in clusters size. The changed electronic structure by QSE have resulted in a number of interesting physicochemical properties, such as single electron tunneling in conductivity, considerable odd-even effect in magnetism, changed color due to surface plasmon and high activity in catalysis. Among them, the effect of electronic structure due to QSE on catalytic activity is unclear yet, because it is very difficult to form finely size-controlled clusters on supports as an essential premise to investigate QSE.

Two main chemical routes have been suggested for the formation of highly dispersed and size-controlled Pt clusters on carbon supports: the colloidal method and impregnation. Several outstanding studies have shown that the colloidal method is a successful way to control the size and shape of clusters. However, eliminating the surface ligands or protectors should be applied to electrocatalysts since the ligands act as surface poisons in electrocatalytic reactions. In contrast, the impregnation method, characterized by the deposition of a precursor followed by a gas or liquid-phase reduction, is simpler and cheaper than the colloidal method. However, with this method it is quite difficult to control the size and dispersity of clusters on the carbon supports, especially those having an inert surface nature, since the affinity of the carbon surface for the precursor solution exerts the dominant effect on dispersity in the deposition step.

To solve such problems, we have recently developed a new cluster formation route based on the fundamental bottom-up approach, namely, SAC (Single Atom to Cluster) approach composed of following two steps, as shown in Figure 1: [1]

1. Form monolayer of single Pt atoms by reducing the Pt precursor (H_2PtCl_6) with $NaBH_4$ on thiolated multi-walled carbon nanotubes (S-MWNT), in which the prepared samples are represented by Pt-S-MWNT.
2. Form Pt clusters from single atoms by eliminating thiol groups with heat treatments at various T_h (Temperature of heat treatment), followed by slow quenching to R.T., in which the prepared samples are represented by $Pt_{h\text{-}q}$/MWNT.

The electronic structure, especially discrete gap of size-controlled Pt clusters formed by SAC approach was investigated with terahertz spectroscopy of BL6B, UVSOR. As can be seen in Figure 2, we have recorded the spectra for Pt clusters supported on MWNT. Pt-S-MWNT is in the state of single Pt atom and the size of $Pt_{h\text{-}q}$/MWNT (T_h=523K) and $Pt_{h\text{-}q}$/MWNT (T_h=873K) is around 1 nm and 4 nm, respectively. The difference of absorption edge around 6 cm^{-1} is clearly shown for Pt-S-MWNT reflecting the fairly different electronic structure from two other samples, although there is little difference between $Pt_{h\text{-}q}$/MWNT (T_h=523K) and $Pt_{h\text{-}q}$/MWNT (T_h=873K). This absorption edge is attributable to the discrete energy level for single Pt atom. However, no discrete level for clusters was observed, because the measurement was conducted room temperature causing thermal excitation. Hence, the experiment at extremely low temperature is required to obtain a clear absorption peak for clusters.

[1] Y.-T. Kim, K. Ohshima, K. Higashimine, T. Uruga, M. Takata, H. Suematsu and T. Mitani, "Fine Size Control of Platinum on Carbon Nanotubes: from Single Atom to Cluster," *Angew. Chem. Int. Ed.*, DOI: 10.1002/anie.200501792, In Press (2005).

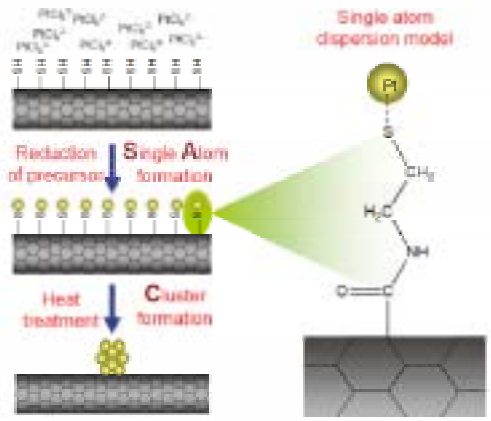

Fig. 1 Scheme of SAC approach.

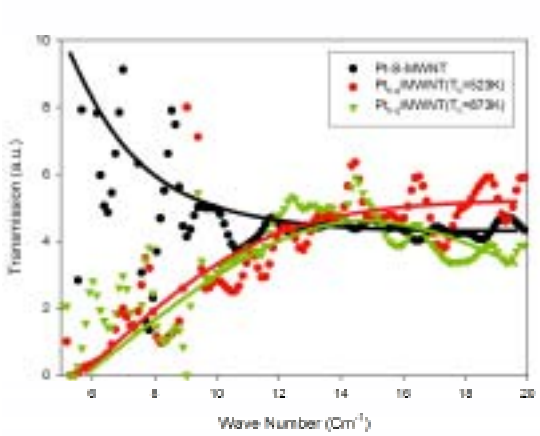

Fig. 2 Terahertz spectroscopy of Pt particles.

BL6B(IR)

Collapse of the Heavy Quasiparticles of $SrFe_4Sb_{12}$ under Magnetic Fields

S. Kimura[1,2], T. Mizuno[2], K. Hayashi[3], E. Matsuoka[3], T. Takabatake[3,4]

[1]*UVSOR Facility, Institute for Molecular Science, Okazaki 444-8585 Japan*

[2]*School of Physical Sciences, The Graduate University for Advanced Studies, Okazaki 444-8585 Japan*

[3]*Department of Quantum Matter, ADSM, Hiroshima University, Higashi-Hiroshima 739-8530, Japan*

[4]*Institute for Advanced Materials Research, Hiroshima University, Higashi-Hiroshima 739-8530, Japan*

Alkaline-earth-filled iron-antimony skutterudites ($A^{2+}Fe_4Sb_{12}$) including $SrFe_4Sb_{12}$ are almost ferromagnetic systems with a paramagnetic Curie temperature (T_C) of 53 K [1]. The origin has been concluded to be the Fe 3*d* spin fluctuation because the thermodynamical properties can be fundamentally explained by the self-consistent renormalization (SCR) theory [2]. However the spin fluctuation is suppressed below 100 K. The origin is considered to be the hybridization between the charge carriers and Fe 3d spins, so-called "Kondo Effect". To clarify it, we measured the magnetic field dependence of optical conductivity spectrum [$\sigma(\omega)$] and derived the effective mass [m^*] and the scattering rate [$1/\tau$] by using the extended Drude model [3].

Obtained magnetic field dependence of $\sigma(\omega)$ at T = 5 K is shown in Fig. 1. $\sigma(\omega)$ shows the pseudogap structure originating from the Fe states [4]. Below the energy gap, the $\sigma(\omega)$ shows the strong magnetic field dependence. This indicates that the Fe 3*d* spins strongly relates to the in-gap state.

The combination of the decreasing direct current conductivity and the change in $\sigma(\omega)$ implies that the heavy-fermion-like electronic structure collapse in the presence of a magnetic field. Due to the extended Drude analysis, m^* of the quasiparticles decreases with increasing magnetic field strength in spite that $1/\tau$ at the accessible lowest photon energy of 2.5 meV does not change as shown in Fig. 2. This is direct evidence of the creation of heavy quasiparticles due to the hybridization between charge carriers and the Fe 3d spins at low temperatures in $SrFe_4Sb_{12}$ and it is suppressed by the magnetic fields.

[1] E. Matsuoka *et al*., J. Phys. Soc. Jpn. **74** (2005) 1382.

[2] K. Ueda and T. Moriya, J. Phys. Soc. Jpn. **39** (1975) 6687.

[3] M. Dressel and G. Grüner, *Electrodynamics of Solids* (Cambridge Univ. Press, Cambridge, 2002).

[4] J. Sichelschmidt *et al.*, Phys. Rev. Lett. **96** (2006) 037406.

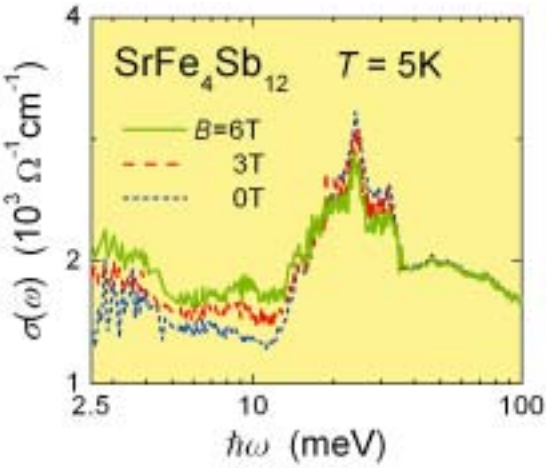

Fig. 1 The magnetic field dependence of optical conductivity spectrum [$\sigma(\omega)$] of $SrFe_4Sb_{12}$.

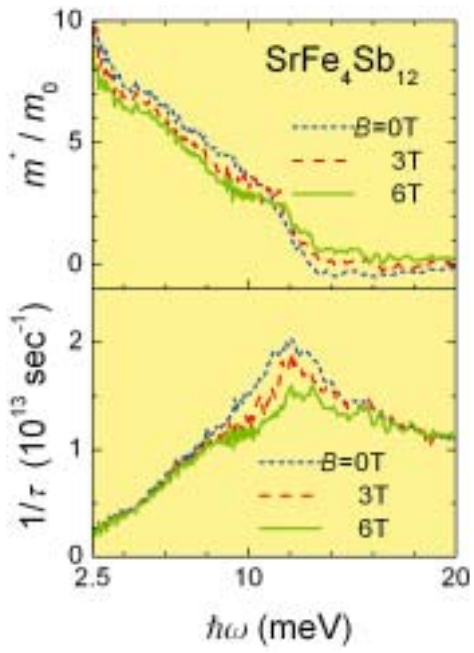

Fig. 2 The magnetic field dependent effective mass relative to the electron rest mass ($m^* = m_0$) and scattering rate ($1/\tau$) as a function of photon energy.

BL6B(IR)&7B

Optical response of $CuRh_2S_4$ & $CuRh_2S_{e4}$

M. Kobayashi[1], K.Satoh[1], A.Irizawa[1], T. Nanba[1], L.Chen[2], M. Ito[3], T. Suzuki[3]
[1]*Kobe University, nada-ku, Kobe 657-8501, Japan*
[2]*ISSP University of Tokyo, 5-1-5 Kashiwanoha, Kashiwa, 277-8581, Japan*
[3]*Hiroshima University,Higashi-Hiroshima 739-8530,Japna*

Introduction

The spinel compound $CuRh_2S_4$ & $CuRh_2S_4$ at atmospheric pressure is a metal of wide temperature range, but undergoes a continuous cross-over change in the electronic states from the metal phase to the insulating phase at high pressures above 5 GPa and 8 GPa, respectively [1]. To study its fundamental electronic states close to the Fermi level ambient pressure, we measured the temperature dependence of optical reflectivity spectra $R(\omega)$ of polycrystalline $CuRh_2S_4$ & $CuRh_2S_4$.

Experimental

The optical reflectivity spectra $R(\omega)$ at ambient pressure was measured in the wide photon energy range from 7 meV to 30 eV in the temperature range of 8-300 K. The measurements were performed using a Fourier-transform interferometer combined with a thermal light source and synchrotron radiation source at the beam line BL6B & 7B of UVSOR. The optical conductivity $\sigma_1(\omega)$and complex dielectric function $\varepsilon_1(\omega)$ were obtained from a standard Kramers-Kronig (K-K) transformation of the measured reflectivity spectrum. $\sigma_1(\omega)$ connected with the absorption spectra by $\sigma_1 = \omega \bullet \varepsilon_2/4\pi$.

Results and discussion

Figure 1 shows the temperature dependences (8 to 300 K) of the σ-spectra of $CuRh_2S_4$ which were obtained from a K-K analysis of the measured $R(\omega)$. In the low energy part of the σ-spectra, two distinct peaks corresponding to electronic interband transitions were resolved at around 0.3 and 0.7eV in addition to the higher energy peaks, together with the small Drude component given by conduction electrons below 0.1 eV. The Drude component still survived even at 8 K.

Figure 2 shows the temperature dependences (8 to 300 K) of the σ-spectra of $CuRh_2S_{e4}$. $CuRh_2Se_4$ exhibits a similar structure with $CuRh_2S_4$ but more clear double peak structure around 0.3 and 0.8 eV (downward arrows). The peak structure becomes distinct accompanying with the growth of the Drude component with cooling at atmospheric pressure.

The weaker temperature dependence and the unresolved broad double peak structure around 0.2-0.8 eV in the σ-spectra of $CuRh_2S_4$ means that the hybridization of the electronic states close to the E_F level is weaker than $CuRh_2S_{e4}$.

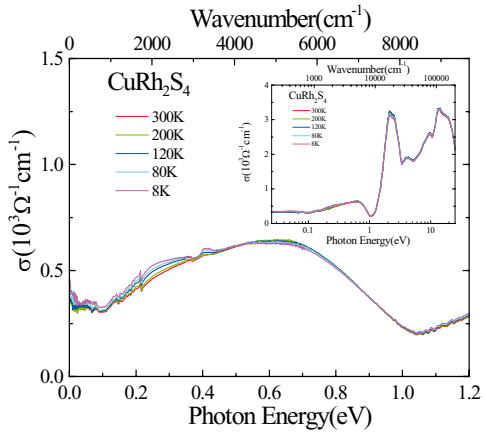

Fig. 1 Temperature dependence of σ-spectra of $CuRh_2S_4$ below 1.2 eV. Insertion indicates the whole spectra up to 30 eV.

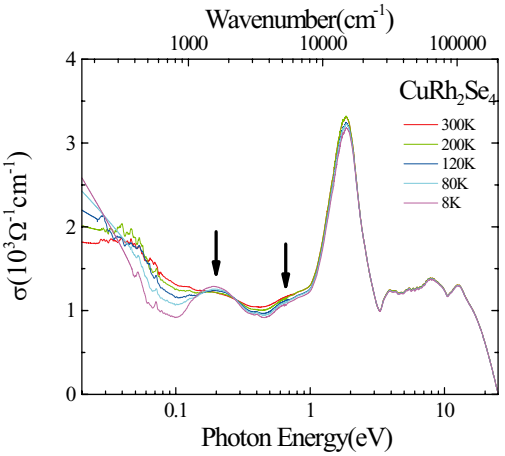

Fig. 2 Temperature dependence of σ-spectra of $CuRh_2S_{e4}$.

[1] M. Ito *et al.*, Phys. Rev. Lett. **91** (2004) 077001.

BL6B(IR)

Infrared Reflection-Absorption Spectroscopy of Alkali-Metal-Doped Alq_3 Thin Films Using Synchrotron Radiation

Y. Sakurai[1], S. Kimura[1], K. Seki[2]

[1]*Institute for Molecular Science, Okazaki 444-8585 Japan*

[2]*Department of Chemistry, Graduate School of Science, Nagoya University 464-8602 Japan*

Tris-(8-hydroxyquinoline) aluminum (Alq_3), which chemical structure and two possible geometrical isomers, meridional (C_1 symmetry) and facial (C_3 symmetry) forms are shown in Figure 1, is most widely used as an electron transport/light emitting layer in organic light emitting diodes (OLEDs). A typical OLED consists of indium tin oxide (ITO) as the anode, on which organic thin films are sequentially deposited, with low work function metals finally deposited as the cathode. Since the OLED's performance is affected by the interface, it is important to investigate the interface between the organic thin film and cathode.

Infrared Reflection Absorption Spectroscopy (IRAS) is a powerful probe for the structure and chemistry of a surface and interface. Though IR spectrum below 1000 cm^{-1} (Far infrared region) is expected to significantly change by the interaction between metal substrate and Alq_3 molecules, it is difficult to obtain the IRAS spectrum in this region using a typical laboratorial system with a globar source. Then we performed the IRAS measurement using synchrotron radiation. In this paper, we report the IRAS spectra of pristine and alkali-metal-doped Alq_3 in the FIR region.

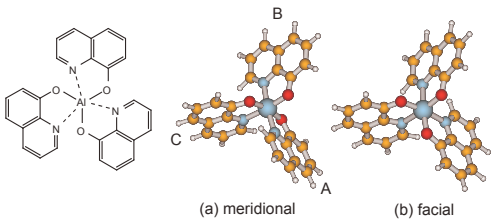

Fig. 1 The chemical structure and geometrical isomers of Alq_3.

Experiments including the sample preparation and measurement were performed in an ultrahigh vacuum chamber. Alq_3 films were prepared by vacuum evaporation onto Ag films deposited on Si substrates. Alkali metals (K, Na, Li) were evaporated from SAES getter sources. IRAS spectra were obtained with the SR light through KBr or CsI windows at the incident angle of 80° relative to the surface normal. The reflected light was detected with a liquid-helium-cooled Si bolometer.

Figure 2 shows the IRAS spectra as a function of the thickness of Alq_3 film in the wavenumber region of 300-500 cm^{-1}. In the spectrum of 1 nm thickness, a peak at 420 cm^{-1} assigned to the Al-N stretching mode was observed. This peak was shifted to 423 cm^{-1}. In addition, a peak at 460 cm^{-1} assigned to the pyramidalization mode was observed in the spectrum of 20 nm thickness. The frequencies of these modes correspond to those of meridional isomer [1]. The lower frequency shift of Al-N stretching mode in the spectrum of 1 nm thickness compared to that of 20 nm thickness is due to the interaction between Alq_3 and Ag surface.

Figure 3 shows potassium doping dependence of the IRAS spectra of an Alq_3 film of 20 nm thickness. The intensity of the peaks at 423 and 460 cm^{-1} gradually decrease and three peaks additionally appear at 435, 441 and 448 cm^{-1} with increasing evaporation amount. The similar behavior was also observed in sodium doping. Considering these behavior, the change is believed to be caused by the charge transfer to the Alq_3 molecule from the alkali atoms. However the additional peaks did not appear in lithium doping. This suggests that the interaction between Li and Alq_3 is different from those of K and Alq_3 and Na and Alq_3.

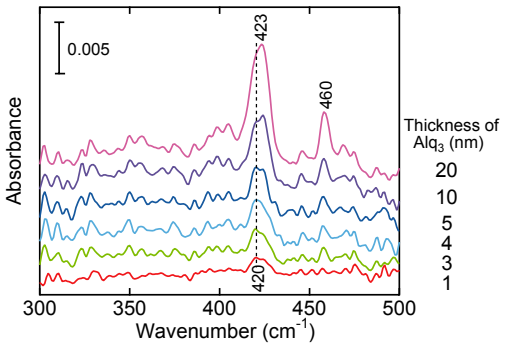

Fig. 2 IRAS spectra as a function of thickness of Alq_3 film.

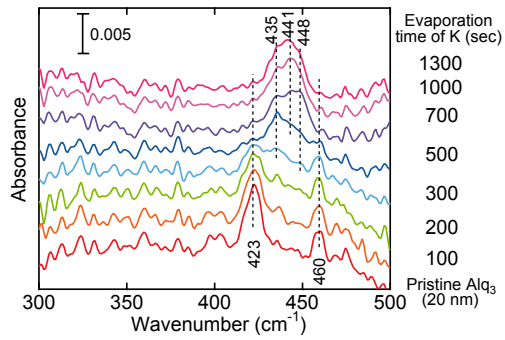

Fig. 3 Changes in IRAS spectra of an Alq_3 film with increasing potassium doping.

[1] M. Cölle, S. Forero-Lenger, J. Gmeiner and W. Brütting, Phys. Chem. Chem. Phys. **5** (2003) 2958.

BL6B(IR)

Metal-Nonmetal Transition of Bismuth Clusters

S. Yoshida, A. Asai, H. Ikemoto
Faculty of Science, University of Toyama, Gofuku 3190, Toyama 930-8555, Japan

A phase transition from Bi nanocrystalline to amorphouslike clusters with decreasing the size is suggested by Raman-scattering measurements [1]. It is very important to investigate the optical property directly to reveal the phase transition. In the present study we report results of optical absorption coefficients for Bi clusters.

Experimental

Bismuth of 99.999 % purity was slowly deposited onto the substrates from a tungsten boat. Then, KBr of 99.99 % purity was deposited to cover the Bi islands. The size of the islands was adjusted by controlling the thickness deposited on the substrates. As mentioned above the Bi clusters are formed in thin films, and samples are represented by their average thickness of the Bi thin films in this paper.

Measurements of optical absorption coefficients were performed in the energy range of 0.05~0.95 eV with the rapid-scan Michelson interferometer (Bruker, IFS-66V) at the IR beam line, BL6B.

Analysis

Figure 1 shows transmittance of the 70 nm-thick film which was on a thick KBr pelette and covered with a 100 nm-thick KBr film. In this report the reference of the transmission is defined by the intensities passed through the KBr pellet.

In the system the transmission is given by

$$T_{calculation} = T_1 \cdot T_2 = \frac{A}{B \cdot C}\exp(-\alpha_2 d_2)$$

$$A = (1-R_{12})^2 + 4R_{12}\sin^2\phi_{12}$$

$$B = 1 + R_{10}R_{12} + \sqrt{R_{10}R_{12}}\cos(\phi_{12} - 2\frac{2\pi n_1 d_1}{\lambda})$$

$$C = (1-R_{12}e^{-\alpha_2 d_2})^2 + 4R_{12}e^{-\alpha_2 d_2}\sin^2(\phi_{12} - \frac{2\pi n_2 d_2}{\lambda}) .$$

Blue line in the Figure 1 shows transmittance calculated by optical constants of crystalline Bi []. The calculated values are in accordance with the experimental values. So we evaluated the absorption coefficients from the experimental data by using the equation 1, where values of A, B and C are calculated by the optical constants of the crystalline Bi. The result is represented by black dots in Figure 2.

Results and Discussion

Figure 2 presents a representative set of curves for the optical absorption coefficients of various thickness films. Several of the characteristics can be seen by examining the absorption data by itself. The absorption coefficients of the 100 nm and 70 nm thick films are close to those of crystalline Bi, suggesting that these films are semimetallic. The absorption coefficients of the 2 nm and 0.5 nm thick films are close to zero around 0.6 eV, and increase linearly with photon energy.

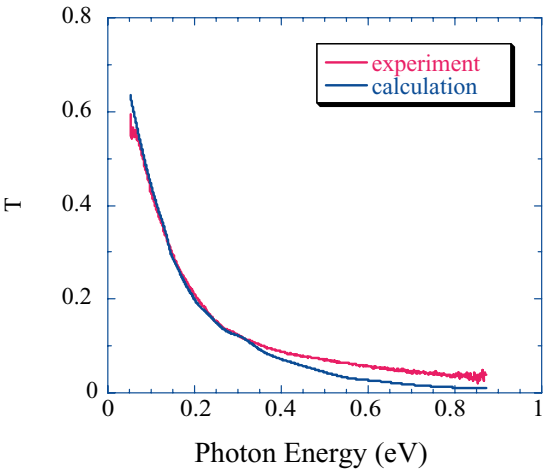

Fig. 1 Transmittance of the 70 nm-thick film.

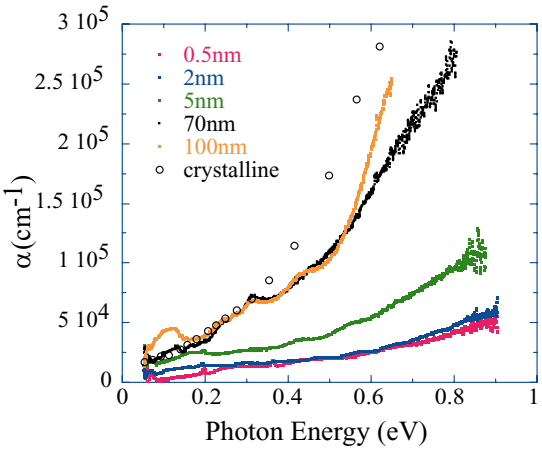

Fig. 2 Variations in optical absorption coefficients of the as-deposited Bi clusters for different thickness. Open circles denote those of polycrystalline [2].

[1] M.G. Mitch, S.J.Chase, J Fortner, R.Q. Yu and J. S. Lannin, Phys. Rev. Lett. **67** (1991) 875.
[2] A.D. Lenham *et al.* J. Opt. Soc. Am. **55** (1965) 1072.

BL7B

Creation Process of Long-Lasting Afterglow in $SrAl_2O_4$:Eu and $SrAl_2O_4$:Eu,Ln (Ln=Dy, Gd, La) Phosphors

M. Kitaura

Fukui National College of Technology, Sabae, 916-8507, Japan

The $SrAl_2O_4$:Eu,Dy phosphor shows an intensive afterglow which lasts for several hours. The function of Dy^{3+} ions has been connected to the formation of photocarrier traps in host $SrAl_2O_4$ [1]. However, it is difficult with only the previous idea to explain the question why the afterglow is enhanced by such co-doping. Thus, the role of Dy^{3+} ions on the afterglow processes still remain unresolved. Since the intensity of afterglow is increased with the concentration of photo-created electrons and holes, the incorporation of Dy^{3+} may influence not only the formation of photocarrier traps but also the change in the absorption feature. In this connection, it is worth while to note the experimental result that the afterglow is efficiently caused with photons in the energy region lower than the fundamental absorption edge of $SrAl_2O_4$ [2]. This suggests the existence of absorption bands resulting from Dy^{3+} co-doping. The origin of the absorption bands has not yet been cleared.

In the present study, we have investigated the creation spectra of afterglow in the phosphors of $SrAl_2O_4$:Eu and $SrAl_2O_4$:Eu co-doped with Dy^{3+}, Gd^{3+} or La^{3+} ions. In order to obtain the creation spectrum of afterglow in each sample, the afterglow spectra were measured at various excitation photon energies by using a grating monochromator with a CCD detector. The creation spectra were corrected for the energy distribution of excitation light source.

The afterglow spectra are dominated by the 2.3 eV band from Eu^{2+} ions. The creation spectra of it in $SrAl_2O_4$:Eu and $SrAl_2O_4$:Eu,Ln (Ln = Dy, Gd, La) are shown in Fig. 1. The spectra were measured at the temperature that the afterglow intensity has the maximum in each sample. The temperatures were 270 K for $SrAl_2O_4$:Eu,Dy and 200 K for others. They exhibit a prominent peak at 6.3 eV. This result indicates that the 6.3 eV peak is not be related to the $4f \rightarrow 5d$ absorption of trivalent Ln ions. In addition, the possibility of the $4f \rightarrow 5d$ absorption band at Eu^{2+} ion is also excluded because the energy position of it does not coincide with that of the 6.3 eV peak. We suppose that the 6.3 eV peak is due to some lattice imperfection. According to Ref. 3, Dy^{3+} ions substitute Sr^{2+} sites. In this case, Sr^{2+} vacancies are necessarily introduced owing to charge compensation. In addition to the Sr^{2+} vacancies, a lot of O^{2-} vacancies should be also produced because all of samples were sintered in a reduced atmosphere. Such vacancies modulate the electronic states of host material, so that the perturbed absorption bands appear in the low energy tail of the fundamental edge. This situation can be seen in the present result.

The cluster calculation has been carried out using the discrete variational $X\alpha$ (DV-$X\alpha$) method [4] to clarify the influence of lattice imperfections on the energy level structure of host $SrAl_2O_4$. From the result of calculations, the intrinsic absorption edge was determined to be 7.73 eV. The agreement between experiment and calculation is good. Now, calculations are proceeding for the cluster introducing a Sr^{2+} or a O^{2-} vacancy.

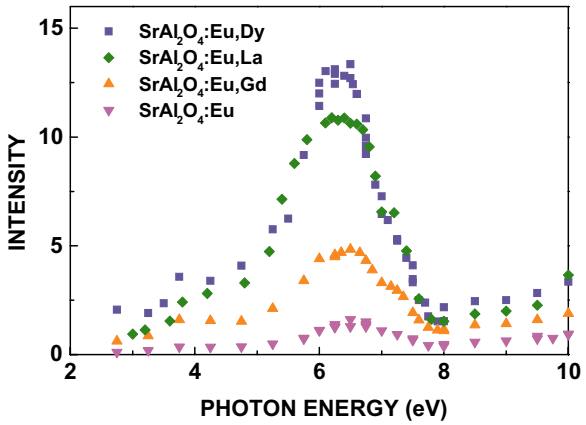

Fig. 1 Creation spectra of the afterglow at 2.3 eV $SrAl_2O_4$:Eu and $SrAl_2O_4$:Eu,Ln (Ln=Dy, Gd, La). The spectra were measured at 270 K for $SrAl_2O_4$:Eu,Dy and at 200 K for others.

[1] T. Matsuzawa, Y. Aoki, N. Takeuchi and Y. Murayama, J. Electrochem. Soc. **143** (1996) 2670.
[2] M. Kamada, J. Murakami and N. Ohno, J. Lumi. **87-89** (2000) 1042.
[3] T. Nakamura, K. Kaiya, N. Takahashi, T. Matsuzawa, C.C. Rowlands, V. Beltran-Lopez, G.M. Smith and P.C. Riedi, J. Mater. Chem. **87-89** (2000) 1073.
[4] H. Adachi, M. Tsukada and C. Satoko, J. Phys. Soc. Jpn. **45** (1978) 875.

BL7B

Vacuum UV Reflectivity Spectroscopy of PZT - Revisited

J. Mistrik[1], M. Aoyama[1], T. Yamaguchi[1], N. Dai[2]

[1]*Research Institute of Electronics, Shizuoka University, Hamamatsu 432-8013 Japan*

[2]*National Laboratory of Infrared Physics, Shanghai Institute of Technical Physics, Chinese Academy of Sciences, Shanghai 200083 China*

The work presented in this report follows up on our ellipsometric and reflectance study performed on $Pb(Zr_{0.5}Ti_{0.5})O_3$ (PZT) film in visible and near UV spectral ranges [1]. It also further refines our previously measured vacuum UV reflectivity data [2], that is important for determination of reliable optical constants of PZT. Forthcoming effort is focused on the development of new dispertion model for this material based on parametrization of the joint density of electronic states in the vicinty of the valence and conduction bands [3, 4].

Experimental

Polycrystalline PZT film was deposited by sol-gel technique on $LaNiO_3$/Pt/Ti/SiO_2/Si substrate. The thickness of PZT and $LaNiO_3$ layers determined by spectroscopic ellipsometry was 217 nm and 100 nm, respectively. UVSOR facility was used for reflectivity measurements. Selected spectral range from 3eV to 30 eV of synchrotron radiation was scanned by 3-m normal incidence monochromator (beam line 7B). Three monochromator gratings G1 (1200 l/mm), G2 (600 l/mm), G3 (300 l/mm) and LiF and quartz filters were used to cover the studied spectral range. Incident and reflected light intensity was measured in room temperature by a Si photodiode. Angle of incidence was less then 15 deg. Reflectivity spectra recorded in step mode with dwelt time approximately 0.2 s, presented here, gave more reliable results with respect to the continuous scan configuration (our spectra presented in Ref. [2]).

Results and Discussions

In the visible range, reflectivity of the sample shows interference fringes due to combined effect of limited thickness and low absorption of PZT film. Knowledge of PZT optical constants determined in the visible range by spectroscopic ellipsometry enabled us to correct the reflectivity data for interference effect. Thus reflectivity of PZT bulk-like sample in vide spectral range (from 1 to 30 eV) was obtained (*c.f.* Fig 1).

Phase of reflectivity coefficient was calculated by Kramers-Kronig relations following numerical procedure reported by Wooten [5]. Extrapolation of reflectivity in low and high photon energy regions was adjusted to obtain best fit between complex refractive index determined from dispersion relations and ellipsometry in visible range. Resulting refractive index and extinction coefficient of PZT film are presented in Fig. 2. Slight deviation of extinction coefficient from zero value in PZT transparence region (1-3 eV) may be due to supplementary reflectance spectral feature located behind 30 eV and therefore unresolved by our experiment.

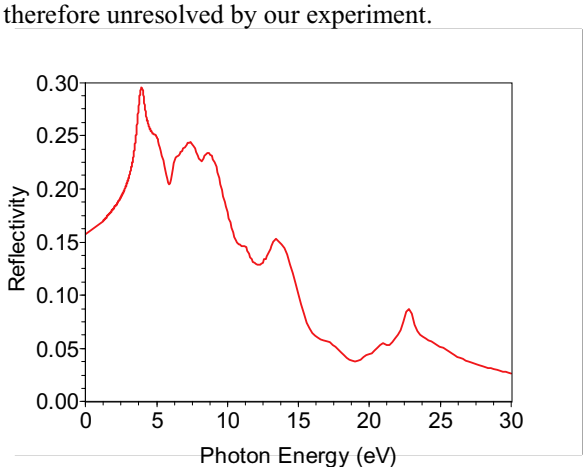

Fig. 1 Reflectivity of PZT.

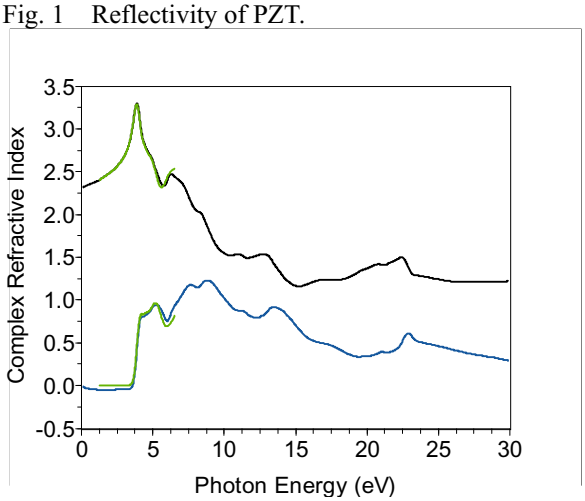

Fig. 2 Refractive index (black line) and extinction coefficient (blue line) of PZT derived from KK analyses of PZT reflectivity spectrum. Corresponding data obtained from ellipsometry are also displayed (green lines).

[1] D. Franta, I. Ohlidal, J. Mistrik, T. Yamaguchi, G. J. Hu, and N. Dai, App. Surf. Sci. **244** (2005) 338.
[2] J. Mistrik, T. Yamaguchi, N. Dai, and M. Shimizu, UVSOR Activity Report 2004 (2005) 87.
[3] D. Franta *et al*. App. Surf. Sci. **244** (2005) 426.
[4] D. Franta, I. Ohlidal, M. Frumar, J. Jedelsky, App. Surf. Sci. **212-213** (2003) 116.
[5] Wooten, Optical Properties of Solids, Academic Press, 1972.

BL7B

Life Time Resolved Photo Luminescence Spectra of UV Emission Bands in AlGaN Alloys

N. Nakagawa[1], K. Fukui[1], S. Naoe[2], H. Miyake[3], K. Hiramatsu[3]

[1]*Research Center for Development of Far-Infrared Region, Fukui University, Fukui910-8507, Japan*

[2]*Faculty of Engineering, Kanazawa University, Kanazawa 920-1192, Japan*

[3]*Faculty of Engineering, Mie University, Mie 514-8507, Japan*

The group III-V nitride semiconductors (AlN, GaN and InN) are promising materials for applications in opt-electronic devices. For ultraviolet LEDs and LDs, the ternary AlGaN alloys are promising semiconductors. We have been performed measurements of visible (VIS)-ultraviolet (UV) photo luminescence (PL) and their excitation spectra (PLE) to investigate PL mechanism of this alloy system [1]. In this report, we present the time resolved decay (TRD) curves profiles for studying the dynamics of this PL.

PL spectra and TRD curves measurements of $Al_xGa_{1-x}N$ (x=0.34~0.76) have been performed under band-to-band excitation region. AlGaN samples were made by MOVPE method at Mie University. The thickness of AlGaN thin films are about 1 μm on 1 μm AlN single crystal film with sapphire substrates. The measurements were carried out at BL7B under single bunch operation in the energy range from 3.4 to 25 eV. Conventional 30 cm VIS-UV monochromator with liquid N_2 cooled CCD detector is used for PL measurements of all samples.

PL spectra of AlGaN are composed of two bands. One is so-called B emission band (UV) which is located near bandedge and corresponding to exciton luminescence, the other is Y emission band (VIS) caused by lattice defects or impurities. Figure 1 shows the time resolved decay curve at each PL energy of UV emission band. Measurement temperature is 9.7 K. TRD curves showed different form at each PL energy position, although all TRD curves are resolved to similar three single exponential components. It suggests that UV emission band consists of three decay components (fast, middle and slow), and each component has different PL energy dependence.

Figure 2 shows PL intensities of three decay components, which are derived from the deconvolutions of all TRD curves in Fig. 1, as functions of PL energies.

These curves give the life time resolved PL spectra. Arrows in Fig.2 indicate the peak energy of each component, and suggest that these three decay components which constitute UV emission band emit with slightly different energies. According to the order of decay times of three components (fast < ns, middle ~ 18ns, slow ~ 80ns), we present consider the fast component as an intrinsic exciton luminescence and the other two components as defect derived ones.

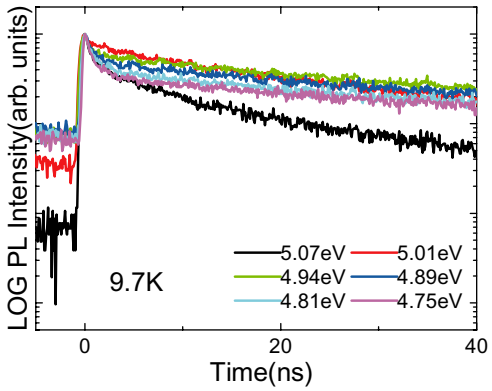

Fig. 1 Time resolved decay curves of $Al_{0.67}Ga_{0.33}N$ at 9.7K.

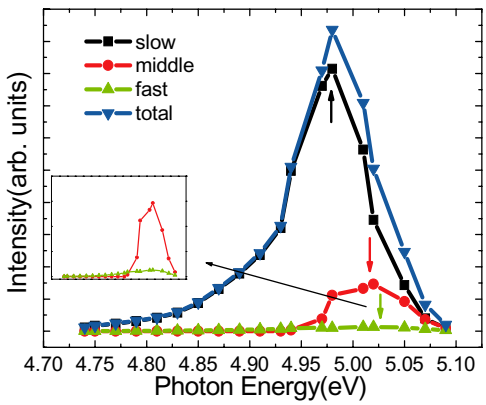

Fig. 2 Life time resolved photo luminescence spectra of $Al_{0.67}Ga_{0.33}N$ at 9.7K.

[1] K. Fukui *et al.*, UVSOR Activity Report 2004 (2005) 78.

BL7B

VUV Reflection Spectroscopy of SiO_2 and SiO_{2-x} Thin Films

K. Nakagawa, T. Tsuda, T. Iwai, Y. Shiraishi, Y. Iwai,
SL. Chang, T. Mizunuma, S. Matsumoto, H. Matsumoto
School of Science & Technology, Meiji University, Kawasaki 214-8571 Japan

Silicon oxide is important material that is used as electronic devices and optical applications. Fundamental studies of silicon oxide are still performed [1]. As optical properties, reflection spectrum of bulk SiO_2 had been report by Philipp *et al.* [2], however those of the thin film of SiO_2 has not been studied. We report the reflection spectra of the thin films of SiO_2 and SiO_{2-x} that are considered as a state with defects of oxygen in the VUV region with synchrotron radiation.

Experimental

SiO_2 and SiO_{2-x} thin films were prepared by RF reactive sputtering. The Si plate with 99.999 % purity was used as a target and the sputtering was carried out in different mixtures of argon and oxygen, under a total pressure of 0.2 Pa. The films were sputtered onto MgF_2 substrate at 573 K. Film thicknesses were about 300 nm. Composition ratio and chemical bonding states of the prepared thin films were investigated by RBS and XPS.

Reflection spectra of SiO_2 and SiO_{2-x} thin films were measured in the vacuum ultraviolet region up to 25.0 eV with the 3-m normal incident monochromator (grating: G1 and G2) at BL-7B of UVSOR-II. And a silicon photodiode sensor was used as a detector for the reflection light.

Results and Discussion

From analyses by RBS and XPS, it was found that the value of x is about 0.5, SiO_2 state and middle state between Si and SiO_2 exist in SiO_{2-x} thin films.

Figure 1 shows the reflection spectra of SiO_2 and SiO_{2-x} thin films at room temperature. Peaks are named as indicated in the figures for convenience. In the spectrum of SiO_2 thin film, five peaks named as A, B, C, D and E were observed at 10.2 eV, 11.8 eV, 14.1 eV, 17.6 eV and 21.7 eV, respectively. This result corresponded with those of absorption spectrum of SiO_2 thin film [3] and reflection spectrum of bulk [2]. In the spectrum of SiO_{2-x}, the peaks corresponding to A~D in the reflection spectrum of SiO_2 thin films could observe, but the peaks became broad in comparison with these of SiO_2 thin film. To clear the structure of the spectra, they were analyzed by secondary derivative method. Figure 2 shows the results. These spectra were normalized as the peak intensity of A accorded with SiO_2 and SiO_{2-x}. From comparison of SiO_2 and SiO_{2-x}, the peak energy of A, C, D, E were shifted about 0.1~0.3 eV, and the peak energy of B was shifted 1.0 eV. Therefore, it seems that the band of the origin of the peak B was influenced by oxygen. From the results of the DV-Xa molecular orbital calculation, the conduction band is consists of the mixed orbital of Si-3s, Si-3p and Si-3d in this region. The band, which is the origin of the reflection peak B may be that the mixed states differ from these of other bands of the origin of the peak A, C, D and E. We expect that the effect of defects of oxygen on electronic structure will be apparent if the cause of the peak shift becomes clear.

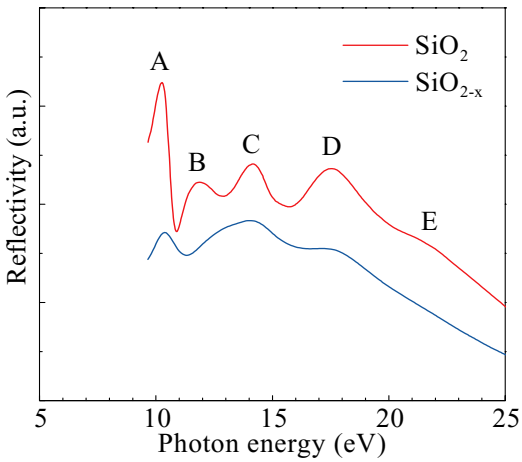

Fig. 1 Reflection spectra of SiO_2 and SiO_{2-x} thin films in the region from 9.5 to 25.0 eV at room temperature.

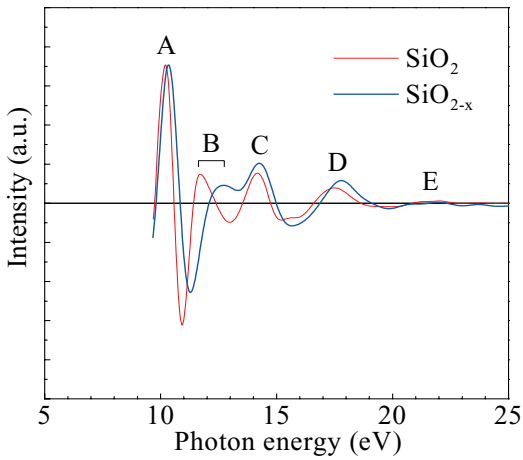

Fig. 2 Normalized secondary derivative spectra of reflection spectra (Fig. 1).

[1] M.P. Seah *et al.*, Surf. Interface Anal. **36** (2004) 1269.
[2] H.R. Philipp, Solid. State. Commun. **4** (1966) 73.
[3] K. Nakagawa *et al.*, UVSOR Activity Report 2004 (2005) 88.

BL7B

Luminescence Properties of YPO_4:Mn Codoped with Zr Ions

Y. Nakajima[1], M. Kitaura[2], M. Kaneyoshi[3], H. Nakagawa[1]
[1]*Dep. of Electrical & Electronics Engineering, Fukui University, Fukui, 910-8507*
[2]*Fukui National College of Technology, Sabae, 916-8507*
[3]*Shin-Etsu Chemical Company, Limited, Takefu Plant, Takefu, 915-8515*

The YPO_4:Mn shows a photoluminescence band peaking at 2.5 eV under excitation with photons in the vacuum ultraviolet (VUV) region at room temeprature. The 2.5 eV emission is enhenced remarkably by co-doping of Zr^{4+} ions.[1] Thus, YPO_4:Zr,Mn is a promising material as functional phosphors for Plasma Display Panels (PDPs) and Hg-free rare-gas discharge lamps. In the present study, photoluminescence properties of YPO_4:Mn, YPO_4:Zr, and YPO_4:Zr,Mn have been investigated at 9.4 and 300 K in order to make clear the role of Zr^{4+} ions on the enhancement in the 2.5 eV emission of YPO_4:Zr,Mn.

The host material YPO_4 was precipitated at 350 K by mixing an aqueous solution of yttrium chloride into a solution of phosphoric acid. The precipitate was filtrate, dried, and calcined in air at 1073K. The YPO_4 powder thus obtained were mixed in a molar together with ZrO_2, MnC_2O_4 and $(NH_4)_2HPO_4$. The mixture was fired in nitrogen flow at 1473K for 3 hours. The concentration of Zr and Mn ions was 2.5 mol% in preparations.

The mesurements of emission and excitation spectra were carried out at BL7B using a 3-m normal incidence monochromator. Photoluminescence from samples was guided into the incident slit of a grating monochromator by a optical fiber, and was detected by a CCD system. The emission spectra presented here were not corrected for the spectral response of detecting system. The excitation spectra were corrected for the spectral distribution of excitation light source.

Figure 1 shows emission spectra of YPO_4:Mn, YPO_4:Zr, and YPO_4:Zr, Mn at 9.4 K (black line) and 300 K (red line). The excitation energy is 7.2eV, which corresponds to the energy of Excimer luminescence by a Xe discharge. In YPO_4:Mn, the emission spectrum at 9.4 K is composed of two band at 2.5 and 1.9eV. This 1.9 eV band is not seen at 300K. The 2.5 eV band is observed at 300 K, though it is very weak. We suppose that the 2.5 and 1.9 eV bands originate in Mn^{2+} ions replacing the Y^{3+} site of YPO_4 lattce, because they are excited in the absorption bands due to the *d-d* transitions of Mn^{2+} ions.

In YPO_4:Zr, two emission bands appear at 4.0 and 3.0 eV. It was found that the 4.0eV band is stimulated with VUV photons in the absorption due to the transitions from O 2*p* states to Zr 4*d* states. Therefore, the 4.0 eV band is most likely assigned to be an emission band associated with Zr^{4+} ions. The 3.0 eV band is observed in YPO_4, so that it may be due to

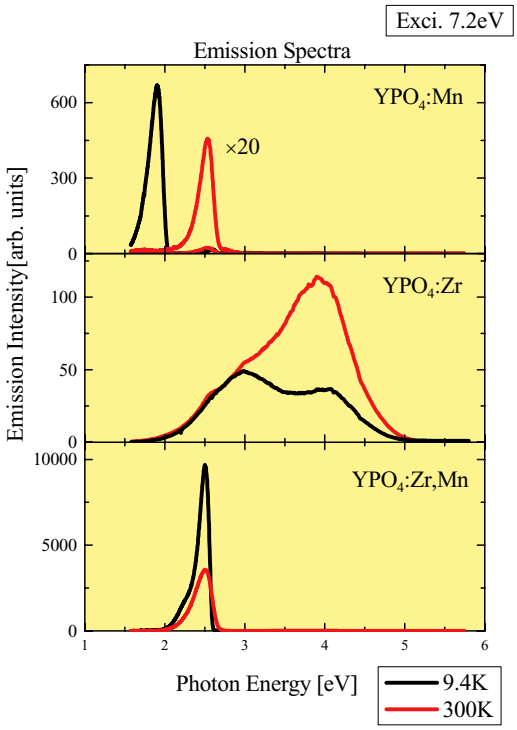

Fig. 1 Emission Spectra of YPO_4:Mn, YPO_4:Zr,and YPO_4:Zr,Mn at 9.4 (black line) and 300 (red line) K.

lattice imperfections in host YPO_4.

The 2.5 eV band dominates the emission spectra of YPO_4:Zr,Mn. The 1.9 eV band of YPO_4:Mn is not seen in the spectra. This result suggests that the electronic states of Mn is influenced by the incorporation of Zr^{4+} ions. Considering the ionic radii of Mn^{2+}, Y^{3+} and P^{5+} ions, Mn^{2+} ions can substitute Y^{3+} ions. On the other hand, since the ionic charge of Mn^{2+} is different from that of Y^{3+}, charge compensation requires to cancel the inconsistency of it between Mn^{2+} and Y^{3+} ions. This effect will introduce vacancies or interstices around Mn^{2+} ions substituting Y^{3+} ions, resulting in an additional perturbation for the electronic states of Mn^{2+}. Such a perturbation should be suppressed by co-doping of Zr^{4+} ions, because the lack of +1 at a Mn^{2+} ion can compensates with the excess of +1 at a Zr^{4+} ion. In this situation, why is the 2.5 eV band enhanced ? This is an open question at present.

[1] M. Kaneyoshi and E. Nakazawa, J. Electrochem. Soc. **152** (2005) H80.

BL7B

Reflectivity of Yb Metal in the Visible, UV and VUV Regions

H. Okamura, K. Senoo, T. Nanba

Graduate School of Science and Technology, Kobe University, Kobe 657-8501, Japan.

The 4*f* electron configuration of Yb in Yb metal is $(4f)^{14}$, hence the valence of Yb is 2+. It has been shown that Yb metal undergoes structural phase transitions with increasing external pressure [1]. At room temperature, the structure changes from fcc at ambient pressure to bcc at about 4 GPa, and to hcp at 26-30 GPa. Below the first transition at 4 GPa, the electrical resistivity of Yb increases with increasing pressure [1]. In addition, the valence of Yb, as probed by X-ray absorption spectroscopy, gradually increases to about 2.7 at 30 GPa [2,3]. When the valence of an Yb ion is 3+, it has a hole within the 4*f* shell; hence it possesses a localized magnetic moment. Namely, as the applied pressure is increased, the number of localized 4*f* holes increases. This can be viewed as a pressure-induced crossover from itinerant to localized character of the 4*f* electrons through the electron-hole symmetry. Associated with this crossover, there should be also changes in the strength of the hybridization between the conduction and 4f electron (*c-f* hybridization). Such characteristics may be viewed as a model system of the so-called ``heavy fermion compounds'', whose pressure-induced physical properties and electronic structures have been under intense research in recent years.

We have recently started infrared studies of Yb metal under external pressure, to probe how the microscopic electronic structures of Yb near the Fermi level evolve with external pressure. To do so, it is also important to study the higher energy optical spectrum, since a wide range of spectrum is required to obtain optical conductivity through the Kramers-Kronig relations. We have measured the reflectivity spectra of Yb metal at room temperature from visible to vuv ranges at BL7B. Since Yb is easily oxidized in air, the sample of Yb metal was prepared by depositing a film of Yb *in situ* on a glass plate by evaporation. A 4N (99.99 %) purity wire of Yb was evaporated with a tungsten filament under a pressure of 4×10^{-9} Torr in the sample chamber.

Figure 1 shows the overall reflectivity spectrum as a function of photon energy. At first, the Yb was deposited onto the glass plate so that we could not see through the glass any more. The reflectivity was first measured at this point, but the spectrum showed a periodic pattern as shown by the red curve. This is due to the interference of the light rays reflected off the front and rear surfaces of the film. This observation demonstrates very well the transparency of metal above the plasma frequency. By analyzing the periodicity of the interference pattern, $nd \sim 50$ nm was obtained (n is the refractive index, d is the thickness). When more Yb was deposited to make the film thickness larger, the interference pattern disappeared (blue curve in Fig. 1). We plan to use this reflectivity data in conjunction with the infrared data taken at Kobe University, to analyze the electronic structures of Yb in the future study.

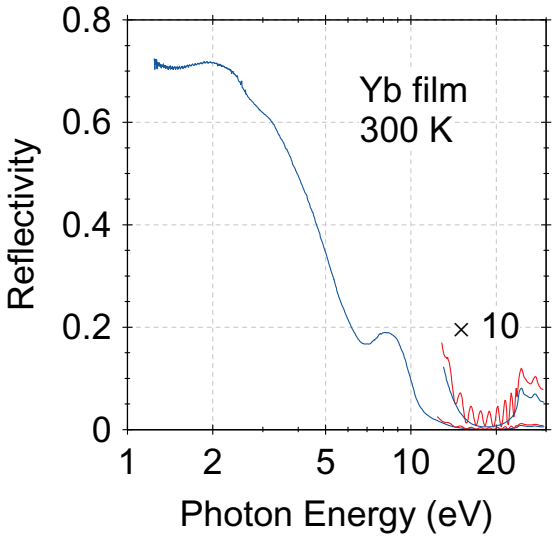

Fig. 1 Reflectivity spectrum of Yb metal at room temperature. The red curve shows the spectrum obtained for a thin film, which shows a periodic pattern due to internal reflection and interference. The blue curve shows the data for a thicker film, which has no interference pattern.

[1] McWhan *et al*., Phys. Rev. **177** (1969) 1063.
[2] Syassen *et al*., Phys. Rev. B **26** (1982) 4745.
[3] Fuse *et al*., J. Alloys Compounds **376** (2004) 34.